Molecular Neurobiology (2025) 62:7183–7204
https://doi.org/10.1007/s12035-025-04713-y

RESEARCH

The Receptor for Advanced Glycation End-products in the Mouse Anterior Cingulate Cortex is Involved in Neuron−Astrocyte Coupling in Chronic Inflammatory Pain and Anxiety Comorbidity

Wei Jiang[1,2] · Minmin Gong[3,4] · Linlin Shen[5] · Chenghui Yu[6] · Huaizhen Ruan[7] · Penghui Chen[7] · Shihao Gao[2] · Zhi Xiao[8,9]

Received: 8 September 2024 / Accepted: 16 January 2025 / Published online: 25 January 2025

Abstract

Previous studies have shown that astrocyte activation in the anterior cingulate cortex (ACC), accompanied by upregulation of the astrocyte marker S100 calcium binding protein B (S100B), contributes to comorbid anxiety in chronic inflammatory pain (CIP), but the exact downstream mechanism is still being explored. The receptor for advanced glycation end-products (RAGE) plays an important role in chronic pain and psychosis by recognizing ligands, including S100B. Therefore, we speculate that RAGE may be involved in astrocyte regulation of the comorbidity between CIP and anxiety by recognizing S100B. Here, we investigated the potential role of RAGE and the correlation between RAGE and astrocyte regulation in the ACC using a mouse model of complete Freund's adjuvant (CFA)-induced inflammatory pain. We detected substantial upregulation of RAGE expression in ACC neurons when anxiety-like behaviors occurred in CFA-treated mice. The inhibition of RAGE expression decreased the hyperexcitability of ACC neurons and alleviated both hyperalgesia and anxiety in CFA-treated mice. Furthermore, we found that the ACC astrocytic S100B level increased over a similar time course. Intra-ACC application of S100B or downregulation of ACC astrocytic S100B via suppression of astrocyte activation significantly affected RAGE levels and the relative behaviors of CFA-treated mice. Taken together, these findings suggest that the upregulation of ACC neuronal RAGE results from the activation of astrocytic S100B and leads to the maintenance of pain perception and anxiety in the late phase after CFA injection, which may partly explain the mechanism by which ACC neuron−astrocyte coupling promotes the maintenance of CIP and anxiety comorbidity.

Keywords Receptor for advanced glycation end-products · S100 calcium binding protein B · Anterior cingulate cortex · Chronic inflammatory pain · Anxiety

Abbreviations

AAV	Adeno-associated virus
ACC	Anterior cingulate cortex
aCSF	Artificial cerebrospinal fluid
AGEs	Advanced glycation end-products
AP	Action potential
ARRIVE	Animal Research: Reporting of In Vivo Experiments
BL	Baseline
CFA	Complete Freund's adjuvant
CIP	Chronic inflammatory pain
CPA	Conditional place avoidance;
DAMPs	Damage-associated molecular patterns
DCA	Distance in the central area
DOA	Distance in the open arms
DRG	Dorsal root ganglion
EGFP	Enhanced green fluorescent protein
ELISA	Enzyme-linked immunosorbent assay;
EPM	Elevated plus maze
FPS-ZM1	4-chloro-N-cyclohexyl-N-(phenylmethyl) benzamide
GFAP	Glial fibrillary acidic protein
HMGB1	High mobility group protein B1
mEPSC	Miniature excitatory postsynaptic currents
L-α-AA	L-alpha-aminoadipic acid
LTP	Long term potentiation
MWT	Mechanical withdrawal threshold
OFT	Open filed test
PAG	Periaqueductal gray
PRR	Pattern-recognition receptors
RAGE	Receptor for advanced glycation end-product

Extended author information available on the last page of the article

RTCA	Retention time in the central area
RTOA	Retention time in the open arms
SDH	Spinal dorsal horn
S100B	S100 calcium binding protein B
TWL	Thermal withdrawal latency
VTA	Ventral tegmental area

Background

The anterior cingulate cortex (ACC) is an important center for pathological pain modulation and receives nociceptive sensory inputs from various cortical and subcortical structures [1], playing a key role in regulating pain and pain-related anxiety [2]. Previous studies have shown that the number of ACC astrocytes can be increased in rodent inflammatory pain models and that the suppression of astrocyte activation can affect pain-related anxiety, depression and aversion [3–5]. However, the exact underlying mechanism is still being explored. S100 calcium binding protein B (S100B) is a member of the S100 protein family and is considered a sensitive and reliable marker of astrocytes that respond to central nervous system damage and disease [6, 7]. S100B can initiate neuronal signaling cascades through paracrine mechanisms to be involved in neuronal synaptic plasticity [8]. It has been shown that S100B is upregulated in activated astrocytes in inflammatory pain model [3, 5]. Therefore, we speculate that the upregulation of astrocytic S100B may play an important role in the neuronal regulation of inflammatory pain comorbid with mood disorders, but the exact mechanism is unclear.

Receptor for advanced glycation end-products (RAGE) is a novel pattern recognition receptor (PRR), and previous studies have shown that RAGE, which is involved in innate immunity, is also expressed on the neurocytic membrane and can participate in oxidative stress by recognizing damage-associated molecular patterns (DAMPs), such as advanced glycation end-products (AGEs), high mobility group protein B1 (HMGB1) and S100B [9–14]. S100B can slowly and continuously activate RAGE and upregulate its expression through positive feedback [3, 7, 15–17]. Many studies have shown that RAGE is involved in the regulation of pain, such as diabetes neuropathic pain [12–14, 18], central post-stroke pain [19], osteoarthritis [20], bone cancer pain [21], and chemotherapy-induced neuropathic pain [10, 22–24]. The upregulation of neuronal RAGE in the dorsal root ganglion (DRG) and spinal dorsal horn (SDH) leads to increased neuronal responsiveness to pain, which is an important cause of hyperalgesia [12, 13]. However, the role of RAGE in chronic pain at the cortical level, especially in the ACC, remains largely unknown. Furthermore, RAGE can also be upregulated in psychiatric disorders such as schizophrenia [25–27], depression [28], and postoperative delirium [29]. It is also unknown whether RAGE is involved in inflammatory pain comorbid with mood disorders.

In this study, we assessed changes in the expression of RAGE in the ACC of chronic inflammatory pain (CIP) model mice and investigated the role of RAGE in the regulation of pain and anxiety-like behaviors. We also explored the correlation between RAGE and astrocyte regulation in the ACC during CIP and tested potential therapeutic methods aimed at RAGE. These findings may partly explain the mechanism by which ACC neuron−astrocyte coupling promotes the maintenance of CIP and anxiety comorbidity and provide some ideas for the development of clinical treatments.

Materials and Methods

Animals

This research was approved by the animal experiment ethics committee of Zunyi Medical University (ZMU21-2306-024). In fact, some previous studies have failed to induce anxiety-like behavior in inflammatory pain mouse models [30, 31]. Given that their studies used only male mice and that both human studies and animal models have shown that females exhibit more severe levels of negative emotion than males do [32, 33], we suspect that mouse sex may be one reason why they did not successfully induce anxiety-like behavior in complete Freund's adjuvant-treated mice. If only female mice are housed together, the oestrus cycle is inhibited because of the absence of male mice and their odor, urine, etc., during the feeding process. This phenomenon is known as the Lee–Booth effect [34]. Therefore, in this study, we used only female mice as subjects.

Female C57BL/6J mice (18–22 g; Beijing Vital River Laboratory Animal Technology Co., Ltd., CN) were maintained on a 12 h light−dark cycle with free access to food and water at a constant room temperature of 24–26°C, with contact with male mice strictly prohibited, thereby suppressing the estrous cycle of female mice and eliminating the influence of hormonal fluctuations through the Lee–Boot effect [34]. All efforts were made to minimize suffering and reduce the number of animals used to the minimum required for statistical accuracy. Every experimental procedure was executed in accordance with the National Institutes of Health Guide for the Care and Use of Laboratory Animals and complied with relevant sections of the Animal Research: Reporting of In Vivo Experiments (ARRIVE) guidelines.

Induction of Inflammatory Pain

Inflammatory pain was induced as previously described [35–38]. The mice were randomized to the experimental or control group and anesthetized with 2% isoflurane (R510-22, RWD Life Science Co., Ltd., CN) and 0.5 L/min O_2 through a small animal anesthesia machine (R500, RWD Life Science Co., Ltd., CN). The mice in the experimental group received an intraplantar injection of 30 μL CFA (F5881, Sigma−Aldrich, DE) on the plantar surface of the left hindpaw. The control mice were injected with an equal volume of 0.9% normal saline (NS).

In Vivo Drug Application

The mice were anesthetized with 2% isoflurane and 0.5 L/min O_2 through a small animal anesthesia machine and then placed into a digital stereotaxic device (68803, RWD Life Science Co., Ltd., CN). Anesthesia was maintained with 0.6% isoflurane and 0.5 L/min O_2 with the bregma and lambda at the same horizontal level. A stainless steel guide cannula with a stainless steel stylet plug (M3.5, RWD Life Science Co., Ltd., CN) was inserted into the ACC (from bregma: anteroposterior 0.7 mm, mediolateral −0.25 mm, dorsoventral −1.1 mm) on the basis of Paxinos and Franklin's Mouse Brain in Stereotaxic Coordinates [39]; 0.5 mm above the injection site, all accessories were sterile. Iodophor was applied to the mice around the incision, and the fresh sterilized bedding was replaced daily to prevent infection after cannula implantation for 4 days. Microinjections were performed on awake mice through a stainless steel injection cannula (M3.5, RWD Life Science Co., Ltd., CN) linked to a single-channel microinjection pump (ZS-KES-II, Beijing Zhongshi Dichuang Technology Development Co., Ltd., CN) via a long flexible pipe. The injection cannula was extended 0.5 mm beyond the tip of the guide cannula, and 500 nL of 5 mM 4-chloro-N-cyclohexyl-N-(phenylmethyl) benzamide (FPS-ZM1, a RAGE-specific inhibitor [40]; HY-19370, MedChemExpress, USA), 10 mM FPS-ZM1, 10 mM L-α-aminoadipic acid (L-α-AA, an astroglial toxin [5]; GC13740, Glpbio Technology Inc., USA) or 0.15 nM S100B (HY-P71276, MedChemExpress, USA) was injected over a 5 min period. The control mice were injected with an equal volume of the corresponding vehicle (containing 0.9% NaCl). The injection cannula was left in place for an additional 5 min and quickly replaced by a stylet plug to minimize the efflux of drugs. The mice were allowed to recover for 15 min before the behavioral experiment.

FPS-ZM1 was first dissolved in 35 μL of DMSO. Then, 90 mg of NaCl and ddH_2O were added to bring the total volume to 1 mL. This resulted in the preparation of isoosmotic 5 mM or 10 mM FPS-ZM1 solutions containing 3.5% DMSO and 0.9% NaCl. The vehicle in the control group also contained 3.5% DMSO and 0.9% NaCl, which corresponded to the groups injected with FPS-ZM1.

L-α-AA or S100B was dissolved in ddH_2O with NaCl, resulting in the preparation of isoosmotic 10 mM L-α-AA or 0.15 nM S100B solutions containing 0.9% NaCl. The vehicle in the control group was NS, which corresponded to the group injected with L-α-AA or S100B.

Behavioral Measurement

Thermal Withdrawal Latency (TWL)

All behavioral experiments were blinded to drug application. The mice were placed separately in a plastic resin test box with a glass bottom and allowed to adapt for 3 h per day for 3 days. The Hargreaves method was used to determine the TWL of the mice [41]. In brief, the beam of a spotlight from the thermal stimulation pain instrument (ZS-PTM, Beijing Zhongshi Dichuang Technology Development Co., Ltd., CN) was focused on the proximal half of the hindpaw plantar surface of the mouse. When the mouse quickly lifted the irradiated hindfoot, the light source was immediately turned off, and the duration of light exposure was recorded. The baseline TWL was established on the day before CFA injection. Each hindpaw was tested three times (with an interval of 10 minutes), and the average value was taken as the TWL. All the mice were subjected to the same intensity of light stimulation, with the protection time set at 40 s to avoid tissue damage.

Mechanical Withdrawal Threshold (MWT)

The mice were placed separately in a plastic resin test box with mesh at the bottom. An isometric force transducer (XH1000, Beijing Zhongshi Dichuang Technology Development Co., Ltd., CN) was connected to the biological signal acquisition and processing system (MiniTR-2, Beijing Zhongshi Dichuang Technology Development Co., Ltd., CN). After the program was set, the filament of the tension transducer was vertically stimulated on the proximal half of the hindpaw plantar surface of the mouse. The pressure gradually increased, and the mouse quickly lifted its foot and completely left the floor, which was considered a positive reaction. The intensity of the filament stimulation was recorded from the MiniTR-2 system. The baseline MWT was established on the day before CFA injection. Each mouse was tested 3 times (with an interval of 10 min), and the average value was taken as the MWT.

Elevated Plus Maze (EPM)

The elevated plus maze included two 50 × 10 cm open arms and two 50 × 10 cm closed arms with 40 cm high walls.

The center of the maze was a 10 × 10 cm open area, and the entire maze was placed at a height of 50 cm. At the beginning of the experiment, the mouse was placed in the center of the maze, with its head facing the open arms. The movement trajectory was recorded within 5 minutes by VisuTrack animal behavior analysis software (XR-VT, Shanghai Xinruan Information Technology Co., Ltd., CN) connected to a camera. The anxiety level of the mice was evaluated via the percentage of retention time in the open arms (RTOA) = [retention time in the open arms/(retention time in the open arms + closed arms)] and percentage of distance in the open arms (DOA) = [distance in the open arms/(distance in the open arms + closed arms)].

Open Field Test (OFT)

A 50 × 50 cm open field was divided equally into 5 × 5 small grids. The middle 3 × 3 grids were considered the central area, while the rest were the surrounding areas. During the experiment, the mouse was placed in a corner of the open field, and VisuTrack animal behavior analysis software was used to record the movement trajectory of the mouse within 5 minutes. The anxiety level of the mice was evaluated via the percentage of retention time in the central area (RTCA) = [retention time in the central area/(retention time in the central area + surrounding area)] and percentage of distance in the central area (DCA) = [distance in the central area/(distance in the central area + surrounding area)].

Immunofluorescence

On the 4th or 9th day after CFA or saline injection, the mice were intraperitoneally injected with 1 mg/kg urethane (U2500, Sigma−Aldrich, DE) for deep anesthesia, followed by cardiac perfusion with 0.01 M PBS and 4% PFA. After perfusion, the right cerebral hemisphere tissue was quickly removed and placed in 4% PFA overnight at 4°C. The brain was subsequently transferred to 4% PFA with 10% sucrose for dehydration until it was submerged to the bottom, and the same procedure was repeated with 30% sucrose. Coronal sections containing the ACC (from bregma: 1.03 ~ 0.40 mm) with a thickness of 30 μm were obtained via a freezing microtome.

For RAGE and NeuN double-labeling immunofluorescence, the brain slices were blocked with blocking solution [3% BSA (A8020, Beijing Solarbio Science & Technology Co., Ltd., CN) + 5% donkey serum (SL050, Beijing Solarbio Science & Technology Co., Ltd., CN) diluted with 0.01 M PBST] for 30 minutes, followed by incubation with rabbit polyclonal RAGE antibody (1:500; ab3611, Abcam, UK) and mouse monoclonal NeuN antibody (1:100; MAB377B, Millipore, USA) diluted with antibody dilution solution (ZLI-9030, Beijing Zhongshan Jinqiao Biotechnology Co., Ltd., CN). The brain slices were incubated at 37°C for 2 hours and then refrigerated at 4°C overnight. After two rinses with 0.01 M PBS and once with 0.01 M PBST, the brain slices were incubated with donkey anti-rabbit Alexa Fluor 568 antibody (1:500; A-10042, Invitrogen, USA) and donkey anti-mouse Alexa Fluor 488 antibody (1:1000; A-21202, Invitrogen, USA) diluted with 0.01 M PBST at room temperature for 2 hours and rinsed with 0.01 M PBS three times. After counterstaining with 1 μg/mL 4,6-diamidino-2-phenylindole (DAPI; D9542, Sigma−Aldrich, DE), the samples were washed with PBS.

For S100B and glial fibrillary acidic protein (GFAP) double-labeling immunofluorescence, a rabbit monoclonal S100B antibody (1:100; ab52642, Abcam, UK) and a mouse monoclonal GFAP antibody (1:500; MAB360, Sigma−Aldrich, DE) were used as primary antibodies and diluted with an antibody dilution solution (ZLI-9030, Beijing Zhongshan Jinqiao Biotechnology Co., Ltd., CN). The donkey anti-rabbit Alexa Fluor 568 antibody (1:500; A-10042, Invitrogen, USA; diluted 1:500 with 0.01 M PBST) and the donkey anti-mouse Alexa Fluor 488 antibody (1:1000; A-21202, Invitrogen, USA) were used as secondary antibodies.

All slices were coverslipped with a mixture of 50% glycerin in PBS and then observed with a spinning disk confocal superresolution microscope (SpinSR10, Olympus, Japan) at 200× magnification. Five slices extracted from a total of 21 consecutive slices containing the ACC (four slices per interval) of each brain were used for immunofluorescence analysis. ImageJ software (NIH, USA) was used to count the red+green fluorescent signal double-labeled cells in each group of images, which represented RAGE+NeuN or S100B+GFAP double-labeled cells. Finally, the numbers of brain slices in each group were averaged, and the units were converted to mm^2.

Enzyme-Linked Immunosorbent Assay (ELISA)

At the designated time points as described above, the mice were intraperitoneally injected with 1 mg/kg urethane (U2500, Sigma−Aldrich, DE) for deep anesthesia. After rapid decapitation, the right half of the ACC tissue was carefully peeled off on an ice box and placed in a grinder. Eukaryotic cell protein lysis solution (5 mL/g; ZD409, Beijing Zoman Biotechnology Co., Ltd., CN) was added to a grinder, and the ACC tissue was crushed for thorough lysis. All steps were carried out on ice. After 10 minutes of lysis, the ACC tissue was centrifuged at 3000 × g at 4°C for 20 minutes, and the supernatant was collected for analysis. The subsequent steps followed the instructions of the mouse RAGE ELISA kit (EK2103, Hangzhou Multiscience Co., Ltd., CN) and mouse S100B ELISA kit (MM-45105M2, Jiangsu Meimian Industrial Co., Ltd., CN). After the color reaction, the optical density (OD) was detected within 30

min to calculate the standard curve and sample concentration via a microplate reader (iMark, Bio-Rad, USA).

In Vivo Plasmid Adeno-Associated Virus (AAV) serotype 2/retro Injection

The mice were anesthetized with 2% isoflurane and 0.5 L/min O_2 through the small animal anesthesia machine and then placed into the digital stereotaxic device, and the anesthesia was maintained with 0.6% isoflurane and 0.5 L/min O_2 as described above. A glass pipette (10–15 μm diameter tip) connected to a nanoliter microinjection pump (R-480, RWD Life Science Co., Ltd., CN) was inserted into the ventral tegmental area (VTA; from bregma: anteroposterior, −3.08 mm; mediolateral, −0.5 mm; dorsoventral, −4.25 mm from skull) or periaqueductal gray (PAG; from bregma: anteroposterior, −3.08 mm; mediolateral, −0.2 mm; dorsoventral, −2.75 mm from skull) according to the mouse brain atlas [39]. A volume of 60 nL of scAAV2/2Retro-hSyn-EGFP-WPRE-pA [5×10^{12} transducing units (TUs); S0581-2R, Shanghai Taitool Bioscience Co., Ltd., CN] was injected over a 1 min period. The injection pipette was left in place for an additional 10 min to minimize the efflux of the virus. Postsurgical animal care was identical to that used for cannula implantation. The mice were killed on day 7 after virus injection as described in a previous study [42] to observe the expression of the virus, and slices of the ACC were subjected to immunofluorescence staining for RAGE. For analysis of the number of EGFP- and RAGE-labeled cells in the ACC, we sampled five slices extracted from a total of 21 consecutive slices containing the ACC (four slices per interval) of each brain (from bregma: 1.03 ~ 0.40 mm). The Image J software was used to count the number of green fluorescent signal and red+green fluorescent signal double-labeled cells throughout the ACC region in the chosen slices in each group of images, which represented EGFP-labeled cells and RAGE+EGFP double-labeled cells, and calculate the ratio of the two numbers.

Whole-Cell Clamp Recordings

For brain slice preparation, at the designated time points, the brains of the mice were quickly removed and submerged at 0°C and preoxygenated (95% O_2, 5% CO_2) in sucrose solution containing the following (in mM): 220 sucrose, 10 D-glucose, 1.25 Na_2HPO_4, 26 $NaHCO_3$, 2.5 KCl, 6 $MgCl_2$, and 1 $CaCl_2$. Coronal slices (300 μm) containing the ACC were prepared via an oscillating tissue slicer (VT1000, Leica, DE), transferred to an incubation chamber filled with artificial cerebrospinal fluid (aCSF) containing the following (in mM): 119 NaCl, 2.5 KCl, 2.5 $CaCl_2$, 1.3 $MgCl_2 \bullet 6H_2O$, 1.25 $NaH_2PO_4 \bullet 2H_2O$, 26.2 $NaHCO_3$, and 11 D-glucose, and aerated with a mixture of 95% O_2−5% CO_2. The room temperature was maintained at 31 to 33°C. After incubation for 90 min, the slices were transferred to a submersion-type recording chamber and perfused with constantly aerated aCSF at a rate of 1–2 mL/min.

Whole-cell recordings were performed in ACC neurons, and the researchers were blinded to the slice preparation. Pyramidal neurons in layer V (right side) were identified [43] via an upright microscope equipped with Leica infrared-differential interference contrast optics, a 340 water-immersion objective, and a charge-coupled device camera. Recording electrodes made from 1.5 mm glass capillaries were pulled on a Flaming-Brown micropipette puller (P-97, Shutter Instrument, USA) and filled with internal solution containing the following (in mM): 145 mM potassium gluconate, 5 HEPES, 0.5 EGTA, 2 $MgCl_2$ and 5 K_2ATP (pH 7.2–7.4). With this solution, the recording electrode exhibited a resistance of 2.5 to 6.0 MΩ. The liquid junction potentials were corrected arithmetically at the beginning of the experiment. After gigaohm seal formation and patch rupture, the series resistance was adjusted to 60 to 80%, and the resistance was continually monitored throughout the experiment. In voltage clamp experiments, capacitive transients are reduced by electronic capacitance compensation in the amplifier circuit. The current clamp recordings were performed in bridge mode. Neurons were allowed to stabilize for at least 5 min before data collection and were discarded if the series resistance increased by more than 20%. The signals were lowpass filtered at 5 kHz via a MultiClamp amplifier (700B, Molecular Devices, LLC., USA), digitized at 10 kHz via a digitizer (1440A, Molecular Devices, LLC., USA) and stored for offline analysis via pClamp9.2 software (Molecular Devices, LLC., USA). The data were analyzed via Clampfit, MATLAB and Excel [1].

Drugs

All the reagents were obtained from Sigma−Aldrich, with the exceptions mentioned above. During whole-cell recording, all the drugs were dissolved in their suitable solvents as stock solutions and were applied by switching the perfusion from aCSF to a solution containing the desired drug at an appropriate concentration. All the stock solutions were stored in tightly sealed vials at −20°C and used within 1 month.

Statistical Analysis

The sample sizes were based on several previous studies and our previous publication [1, 30, 41, 44, 45]. All the quantitative values were normally distributed and are expressed as the means ± SDs. All comparisons between the two groups were analyzed via Student's unpaired t tests. One-way ANOVA, followed by post hoc Bonferroni

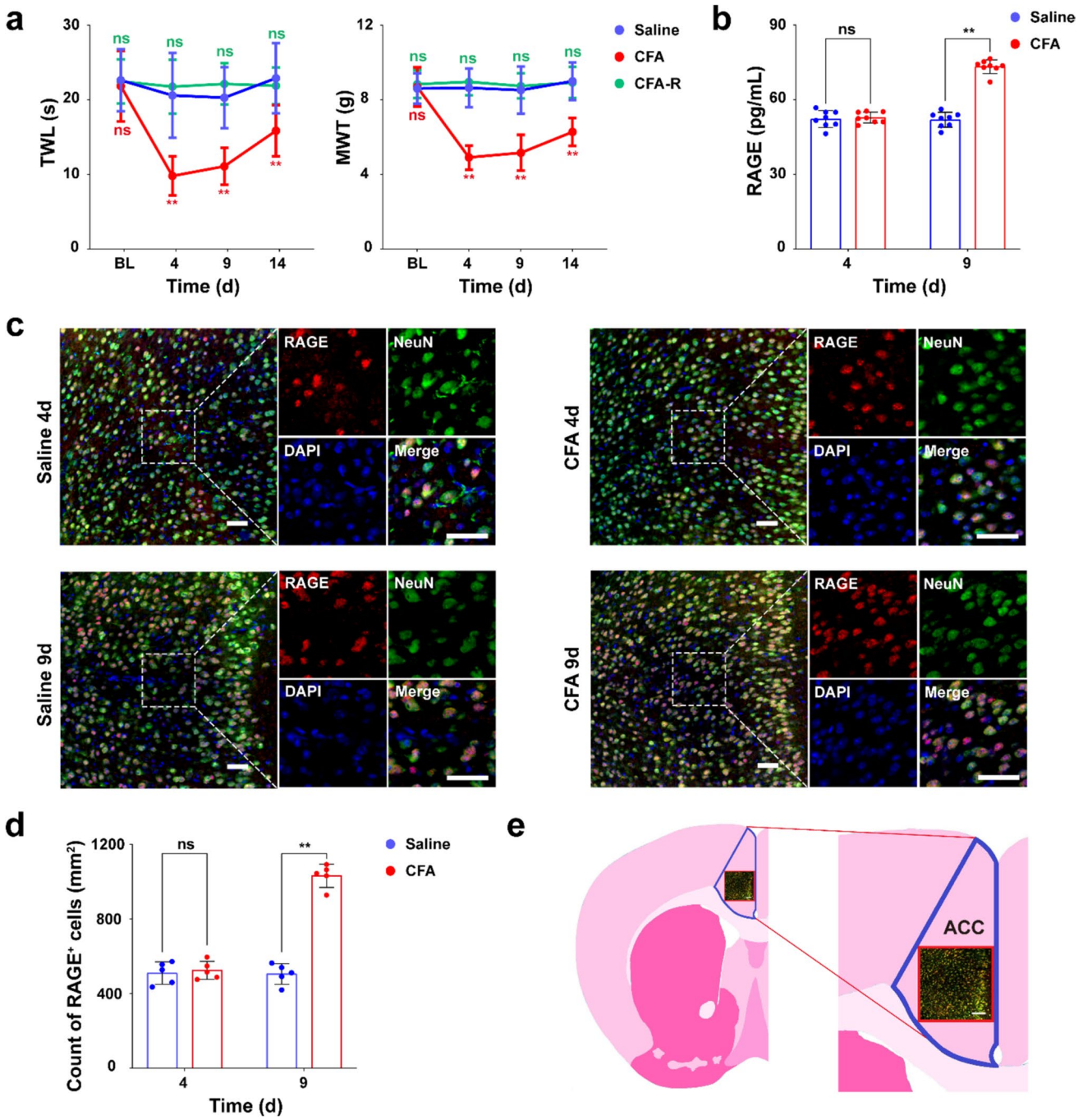

Fig. 1 RAGE expression in the ACC is upregulated at 9d after CFA treatment. **a**, Progression of the thermal withdrawal latency (TWL) and mechanical withdrawal threshold (MWT) following intraplantar CFA or saline injection. CFA-R: the right hindpaws of CFA-treated mice contralateral to the CFA injection. BL: baseline. **b**, Expression level of RAGE in the ACC at different stages after intraplantar CFA or saline injection, as measured by ELISA. **c**, Immunofluorescence of RAGE in ACC neurons at different stages after intraplantar CFA or saline injection (scale bar = 50 μm). **d**, Count numbers of RAGE-positive neurons. **e**, Schematic diagram showing where the immunofluorescence images were taken. ** $p < 0.01$. ns: not significant

multiple comparison tests, was used for three or more sets of data. Changes in the TWL and MWT in the time course experiments were measured via two-way repeated-measures ANOVA. The Kruskal−Wallis H test was used to compare the rheobase grades. Statistical comparisons were made via SPSS version 19 software (SPSS Inc., USA). In all cases, $p < 0.05$ (two-tailed test) was considered to indicate statistical significance.

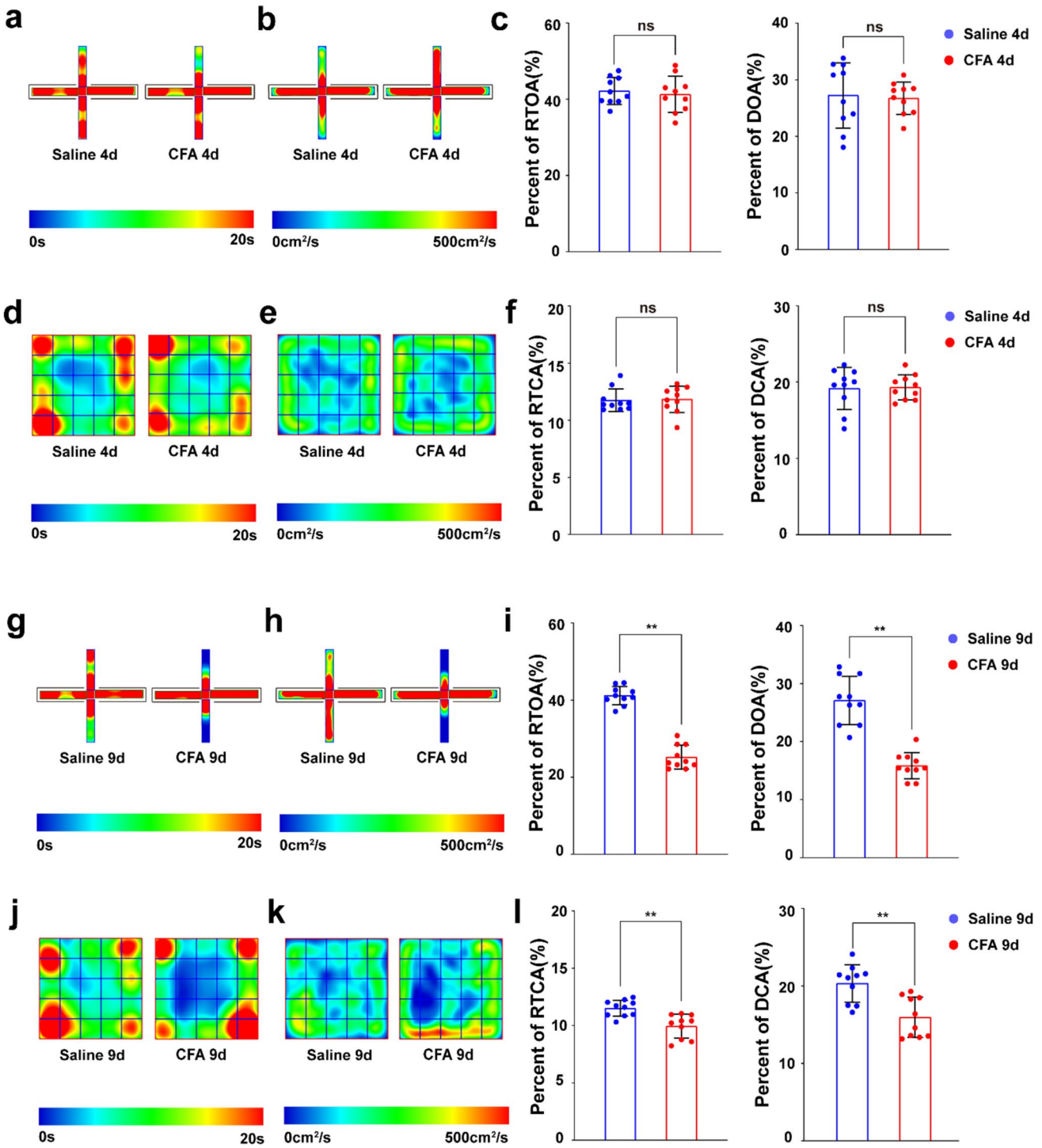

Fig. 2 Anxiety-like behavior occurs at 9d after CFA treatment. **a**, **b**, Heatmap (a) and activity map (b) of mice in the elevated plus maze on day 4 after saline or CFA injection (the cross arm of the map is the closed arm, and the longitudinal arm is the open arm). **c**, Calculation of the percentage of time spent in the open arm (RTOA) and the percentage of distance traveled in the open arm (DOA) by the mice in the elevated plus maze. **d**, **e**, Heatmap (d) and activity map (e) of mice in the open field test on day 4 after saline or CFA injection. **f**, Calculation of the percentage of mouse retention time in the central area (RTCA) and the percentage of mouse distance traveled in the central area (DCA) in the open field test. **g**, **h**, Heatmap (g) and activity map (h) of mice in the elevated plus maze on day 9 after saline or CFA injection (the cross arm of the map is the closed arm, and the longitudinal arm is the open arm). **i**, The percentage of time spent in the open arm (RTOA) and the percentage of distance traveled in the open arm (DOA) by the mice in the elevated plus maze were calculated. **j**, **k**, Heatmap (j) and activity map (k) of mice in the open field test on day 9 after saline or CFA injection. **l**, Calculation of the percentage of mouse retention time in the central area (RTCA) and the percentage of mouse distance traveled in the central area (DCA) in the open field test. * $p < 0.05$, ** $p < 0.01$. ns: not significant

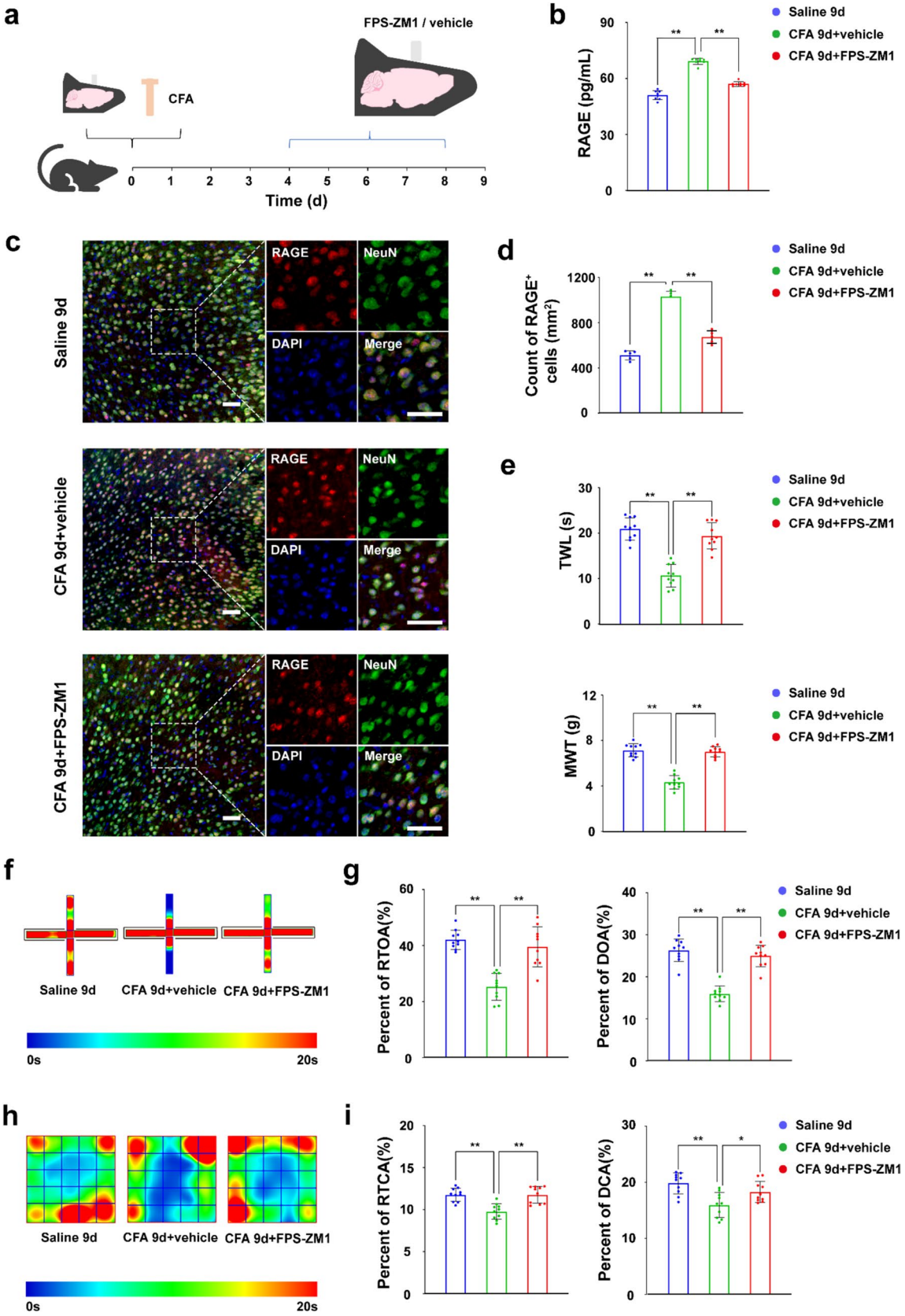
a
FPS-ZM1 / vehicle
CFA
0 1 2 3 4 5 6 7 8 9
Time (d)
b
RAGE (pg/mL)
90
60
30
0
**
**
Saline 9d
CFA 9d+vehicle
CFA 9d+FPS-ZM1
c
Saline 9d
CFA 9d+vehicle
CFA 9d+FPS-ZM1
RAGE
NeuN
DAPI
Merge
d
Count of RAGE+ cells (mm2)
1200
800
400
0
e
TWL (s)
30
20
10
0
MWT (g)
12
8
4
0
f
Saline 9d
CFA 9d+vehicle
CFA 9d+FPS-ZM1
0s
20s
g
Percent of RTOA(%)
60
40
20
0
Percent of DOA(%)
40
30
20
10
0
h
Saline 9d
CFA 9d+vehicle
CFA 9d+FPS-ZM1
0s
20s
i
Percent of RTCA(%)
20
15
10
5
0
Percent of DCA(%)
30
20
10
0
*

◂**Fig. 3** Intra-ACC injection of FPS-ZM1 decreases RAGE expression and alleviates hypersensitivity and anxiety in CIP mice. **a**, Schematic diagram showing where and when FPS-ZM1 or vehicle was injected. **b**, Expression level of RAGE in the ACC, including the saline control group and CFA groups, after FPS-ZM1 or vehicle injection, as measured by ELISA. **c,** Immunofluorescence of RAGE in ACC neurons from the saline control group and the CFA groups after FPS-ZM1 or vehicle injection (scale bar = 50 μm). **d**, Count numbers of RAGE-positive neurons. **e**, Thermal withdrawal latency (TWL) and mechanical withdrawal threshold (MWT), including those of the saline control group and the CFA groups after FPS-ZM1 or vehicle injection. **f**, Heatmap of the elevated plus maze, including the saline control group and the CFA groups, after FPS-ZM1 or vehicle injection (the cross arm of the map is the closed arm, and the longitudinal arm is the open arm). **g**, Calculation of the percentage of time spent in the open arm (RTOA) and the percentage of distance traveled in the open arm (DOA) by the mice in the elevated plus maze. **h**, Heatmap of the open field test results, including those of the saline control group and the CFA groups, after FPS-ZM1 or vehicle injection. **i**, Calculation of the percentage of mouse retention time in the central area (RTCA) and the percentage of mouse distance traveled in the central area (DCA) in the open field test. * $p < 0.05$, ** $p < 0.01$

Results

RAGE Expression is Upregulated in the ACC when Anxiety-Like Behaviors Occur and Hyperalgesia Persists

To explore the changes in RAGE expression in the ACC during CIP, we established an inflammatory pain model by intraplantar injection of CFA in C57BL/6J mice, as previously described. The same volume of saline was intraplantarly injected as a control.

After CFA injection, the TWL and MWT of the injected hindpaw significantly decreased within 4 days and lasted at least 9−14 days (two-way repeated-measures ANOVA: TWL: main effect of group $F_{(2)} = 33.41$, $p < 0.001$; MWT: main effect of group $F_{(2)} = 96.34$, $p < 0.001$; all groups $n = 10$ mice; Fig. 1a), which is consistent with the previous

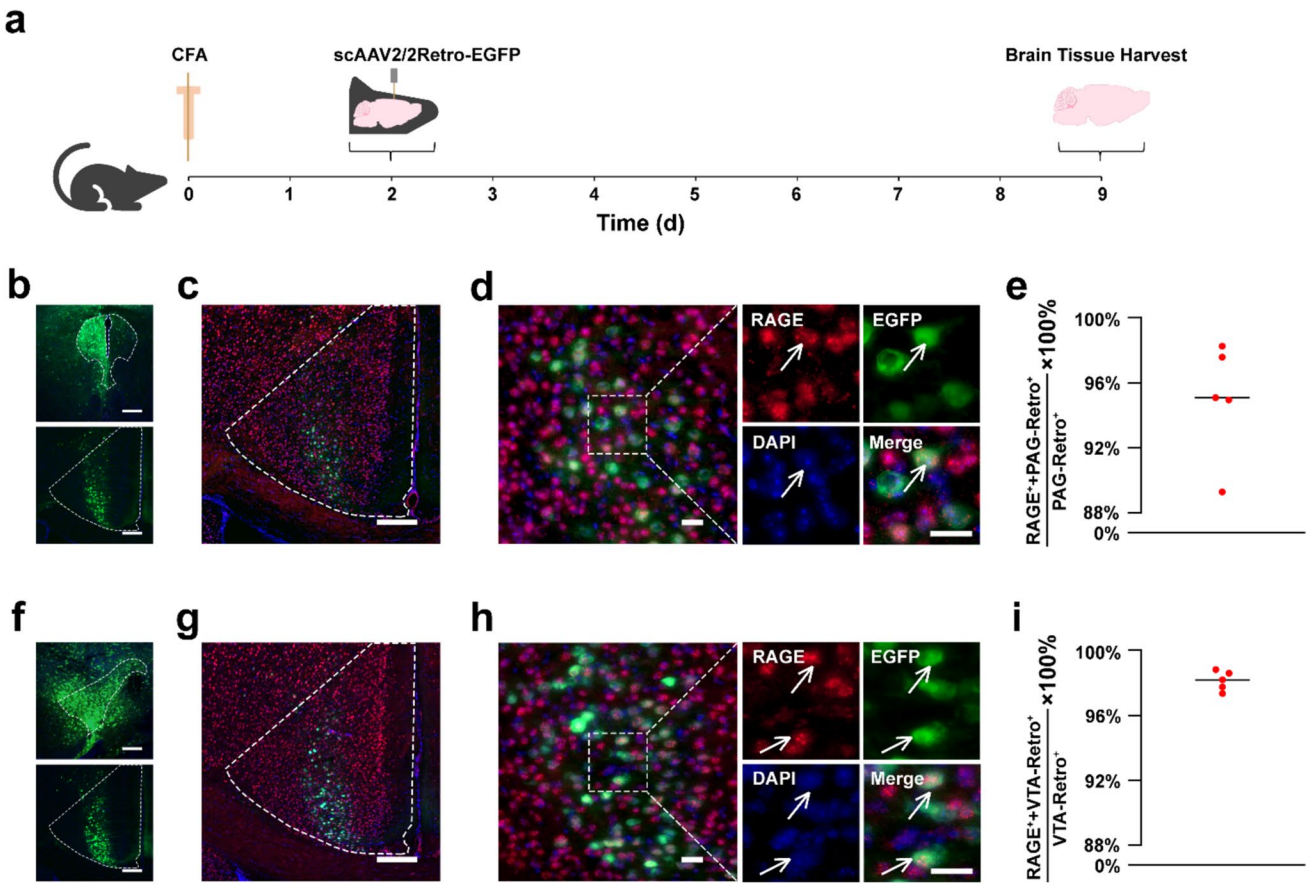

Fig. 4 RAGE is expressed on ACC neurons that project to the PAG and VTA. **a**, Schematic diagram showing when scAAV2/2retro-EGFP was injected. **b**, Injection site of scAAV2/2retro-EGFP in the PAG (upper panel) and retrogradely labeled cell bodies in the ACC (lower panel) (scale bar = 200 μm). **c**, Immunofluorescence of RAGE (red) and scAAV2/2retro-EGFP (green) in ACC neurons (scale bar = 200 μm). **d**, Enlarged view of RAGE-positive ACC neurons labeled with scAAV2/2retro-EGFP injected into the PAG (scale bar = 25 μm). **e**, Ratio of the number of RAGE+PAG-Retro-EGFP double-positive cells to PAG-Retro-EGFP positive cells. **f**, Injection site of scAAV2/2retro-EGFP in the VTA (upper panel) and retrogradely labeled cell bodies in the ACC (lower panel) (scale bar = 200 μm). **g**, Immunofluorescence of RAGE (red) and scAAV2/2retro-EGFP (green) in ACC neurons (scale bar = 200 μm). **h**, Enlarged view of RAGE-positive ACC neurons labeled with scAAVretro-EGFP injected into the VTA (scale bar = 25 μm). **i**, Ratio of the number of RAGE+VTA-Retro-EGFP double-positive cells to VTA-Retro-EGFP positive cells

description of this chronic pain model. Next, we explored the expression level of RAGE in the ACC at 4 and 9 days after CFA or saline injection via ELISA and immunofluorescence methods. At the early stage after CFA or saline injection, i.e., 4 days after injection, the protein levels of RAGE (one-way ANOVA: $F_{(3,28)} = 106.583$, $p < 0.001$; post hoc Bonferroni correction: Saline 4d vs CFA 4d: $p = 1.000$; all groups $n = 8$ biological replicates; Fig. 1b) and RAGE-positive cell numbers (one-way ANOVA: $F_{(3,16)} = 104.648$, $p < 0.001$; post hoc Bonferroni correction: Saline 4d vs CFA 4d: $p = 1.000$; all groups $n = 5$ mice; Fig. 1c-d) in the ACC were not significantly different between the two groups. However, at the late stage after injection (day 9), the protein levels of RAGE (one-way ANOVA: post hoc Bonferroni correction: Saline 9d vs CFA 9d: $p < 0.001$) and the number of RAGE-positive cells (one-way ANOVA: post hoc Bonferroni correction: Saline 9d vs CFA 9d: $p < 0.001$) in the ACC were markedly greater in the CFA group than in the saline group (Fig. 1b-d). These results revealed that the upregulation of RAGE in the ACC occurred at the late stage, but not the early stage, of CIP.

We also detected anxiety-like behaviors after CFA injection. The elevated plus maze and open field tests were used to evaluate the degree of anxiety of the mice. We found

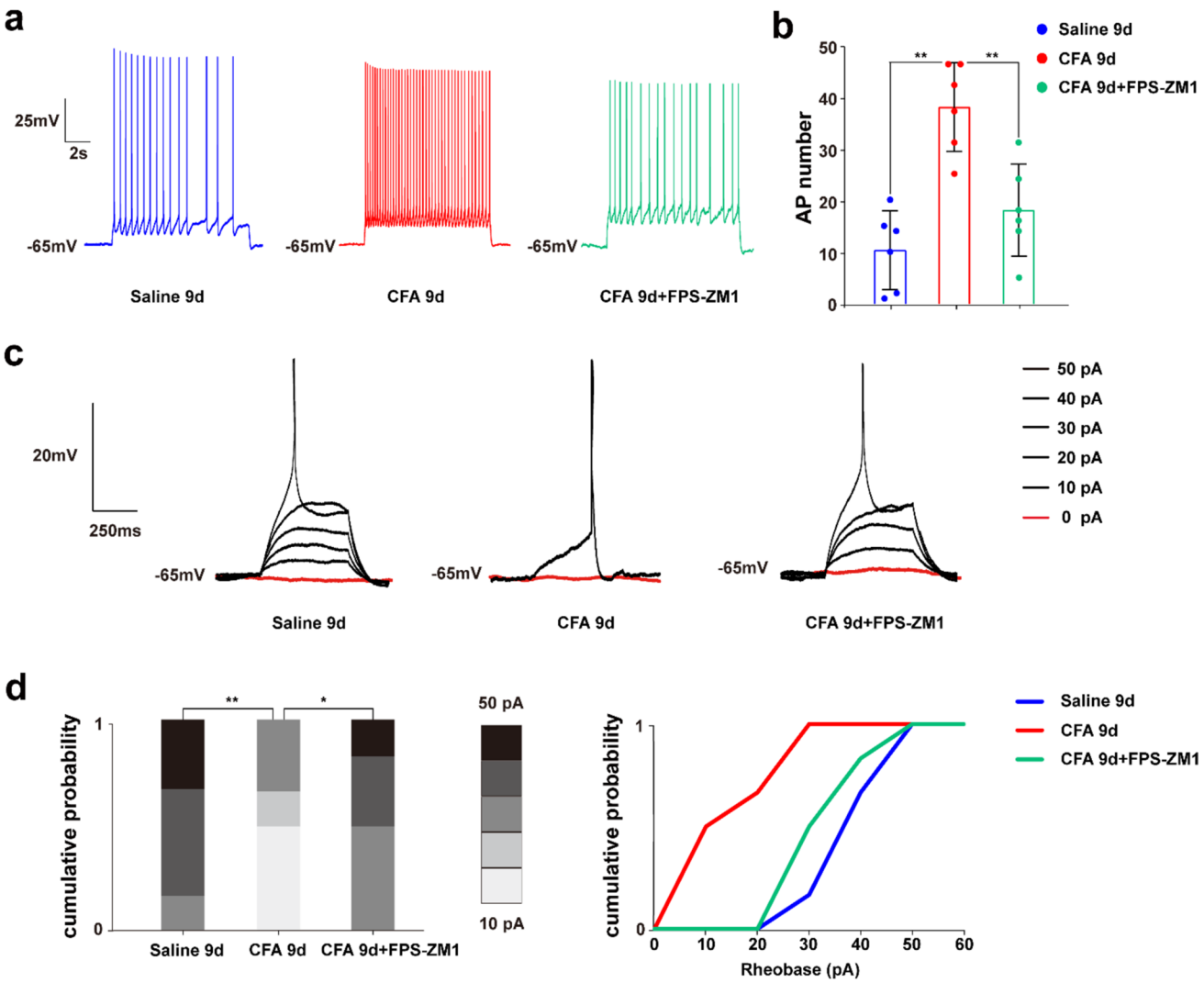

Fig. 5 Inhibition of RAGE alleviated hyperexcitability of ACC neurons at the late stage of CIP. **a**, Representative traces showing the firing response of ACC neurons in the Saline 9d, CFA 9d and CFA 9d+FPS-ZM1 groups to a 10-s 50 pA stimulus. **b**, Statistical comparison of the number of APs in the three groups in (a). **c**, Representative traces of evoked responses elicited by the application of 300 ms depolarizing current pulses from 0 to +50 pA (step = 10 pA) in Saline 9d, CFA 9d and CFA 9d+FPS-ZM1 neurons. The red line represents the response at 0 pA. The traces of each neuron were interrupted when the 1st AP was observed. **d**, Number of neurons at each rheobase grade and the cumulative probability curve chart in the Saline 9d, CFA 9d and CFA 9d+FPS-ZM1 groups. * $p < 0.05$, ** $p < 0.01$. ns: not significant

that on day 4 after CFA injection, the percentage of retention time in the open arm (RTOA) and the percentage of distance traveled in the open arm (DOA) in the CFA group were similar to those in the saline group (unpaired Student's t test: RTOA: $t_{(18)} = 0.678$, $p = 0.638$; DOA: $t_{(18)} = 0.067$, $p = 0.947$; all groups $n = 10$ mice; Fig. 2a-c). These results indicated that the mice in the CFA group and saline group spent equal amounts of time exploring the open arms on day 4. In the open field test, mice in the saline and CFA groups also presented a similar percentage of retention time in the central area (RTCA) and a similar percentage of distance traveled in the central area (DCA) (unpaired Student's t test: RTCA: $t_{(18)} = -0.189$, $p = 0.852$; DCA: $t_{(18)} = -0.120$, $p = 0.906$; all groups $n = 10$ mice; Fig. 2d-f), suggesting that compared with normal mice, CFA-treated mice spent equal amounts of time in the central area. These results indicated that CFA-treated mice did not exhibit anxiety on day 4. However, on day 9 after intraplantar CFA injection, anxiety-like behaviors were much more prominent. Compared with the saline-treated mice, the CFA-treated mice spent much less time exploring the open arms in the elevated plus maze, as reflected by a lower percentage of RTOA and DOA (unpaired Student's t test: RTOA: $t_{(18)} = 13.066$, $p < 0.001$; DOA: $t_{(18)} = 9.479$, $p < 0.001$; all groups $n = 10$ mice; Fig. 2g-i). Similarly, compared with the saline-treated mice, the CFA-treated mice spent much less time in the central area of the open field, as reflected by a lower percentage of the RTCA and DCA (unpaired Student's t test: RTCA: $t_{(18)} = 3.919$, $p = 0.001$; DCA: $t_{(18)} = 3.894$, $p = 0.001$; all groups $n = 10$ mice; Fig. 2j-l). Taken together, our results suggest that anxiety mainly occurs at the late stage of CIP.

Inhibition of RAGE Alleviated Both the Hyperalgesia and Anxiety-Like Behaviors of CIP

Thus, we wondered whether the inhibition of RAGE could modulate chronic pain-related behaviors. Therefore, we intra-ACC microinjected the RAGE-specific inhibitor FPS-ZM1 from day 4 to day 8 after intraplantar CFA injection to inhibit the upregulation of RAGE (Fig. 3a). Intra-ACC microinjection of vehicle was used as a control. On day 9 after CFA model establishment, the ELISA and immunofluorescence results confirmed that RAGE protein levels (unpaired Student's t test: $t_{(14)} = 16.631$, $p < 0.001$; all groups $n = 8$ biological replicates) and RAGE-positive neuron numbers (unpaired Student's t test: $t_{(8)} = 11.013$, $p < 0.001$; all groups $n = 5$ mice) were significantly decreased by FPS-ZM1 (Fig. 3b-d). Additionally, the CFA-treated mice that received intra-ACC FPS-ZM1 injection presented greater TWL and MWT values on day 9 after CFA model establishment than did those that received intra-ACC vehicle injection did (unpaired Student's t test: TWL: $t_{(18)} = -7.264$, $p < 0.001$; MWT: $t_{(18)} = -11.608$, $p < 0.001$; all groups $n = 10$ mice; Fig. 3e).

To explore the effects of FPS-ZM1 on anxiety-like behaviors, we also conducted elevated plus-maze and open field tests on day 9 in the CFA model. As expected, the CFA-treated mice that received intra-ACC FPS-ZM1 injection spent significantly more time and traveled longer distances in the open arm of the elevated plus maze (unpaired Student's t test: RTOA: $t_{(18)} = -5.332$, $p < 0.001$; DOA: $t_{(18)} = -9.105$, $p < 0.001$; all groups $n = 10$ mice; Fig. 3f-g) and in the central area of the open field (unpaired Student's t test: RTCA: $t_{(18)} = -4.623$, $p < 0.001$; DCA: $t_{(18)} = -2.562$, $p = 0.020$; all groups $n = 10$ mice; Fig. 3h-i) than did the CFA-treated mice that received intra-ACC vehicle injection. These results suggest that the upregulation of RAGE expression is involved in the progression of inflammatory pain and the comorbidity of anxiety. In addition, we found that the therapeutic effect of FPS-ZM1 on the behavior of CFA-treated mice was dose dependent, as the effect of 5 mM FPS-ZM1 was significantly weaker than that of 10 mM FPS-ZM1 (Supplementary Fig. 1).

RAGE is Expressed on ACC Neurons that Project to Nuclei, which Modulates Pain Sensation and Pain-Related Anxiety

Given that downregulation of RAGE expression rescued both hypersensitivity and anxiety, we explored the cellular expression pattern of RAGE in the ACC. Previous studies have shown that ACC neurons with specific projection targets perform different functions. The ACC-PAG projection mainly modulates pain sensation [46], whereas the ACC-VTA projection modulates the emotional comorbidities of chronic pain, such as anxiety [41, 47]. Thus, we injected retrograde AAV (scAAV2/2Retro-EGFP) into the PAG or VTA (Fig. 4a-b and f) on day 2 after CFA injection. The mice were killed on day 7 after virus injection on the basis of a previous study [42] (day 9 after CFA injection) to observe the expression of the virus, and ACC slices were subjected to immunofluorescence staining of RAGE in the ACC (Fig. 4c and g). Most of the PAG-projecting ACC neurons were labeled with RAGE (the ratio of the number of RAGE+PAG-Retro-EGFP double-positive cells to PAG-Retro-EGFP positive cells was 95.02%±3.53%; $n = 5$ mice; Fig. 4d and e). Similarly, most VTA-projecting ACC neurons were labeled with RAGE (the ratio of the number of RAGE+VTA-Retro-EGFP double-positive cells to the number of VTA-Retro-EGFP positive cells was 98.12%±0.61%; $n = 5$ mice; Fig. 4h and i). Therefore, inhibition of RAGE might simultaneously regulate the function of PAG-projecting and VTA-projecting ACC neurons.

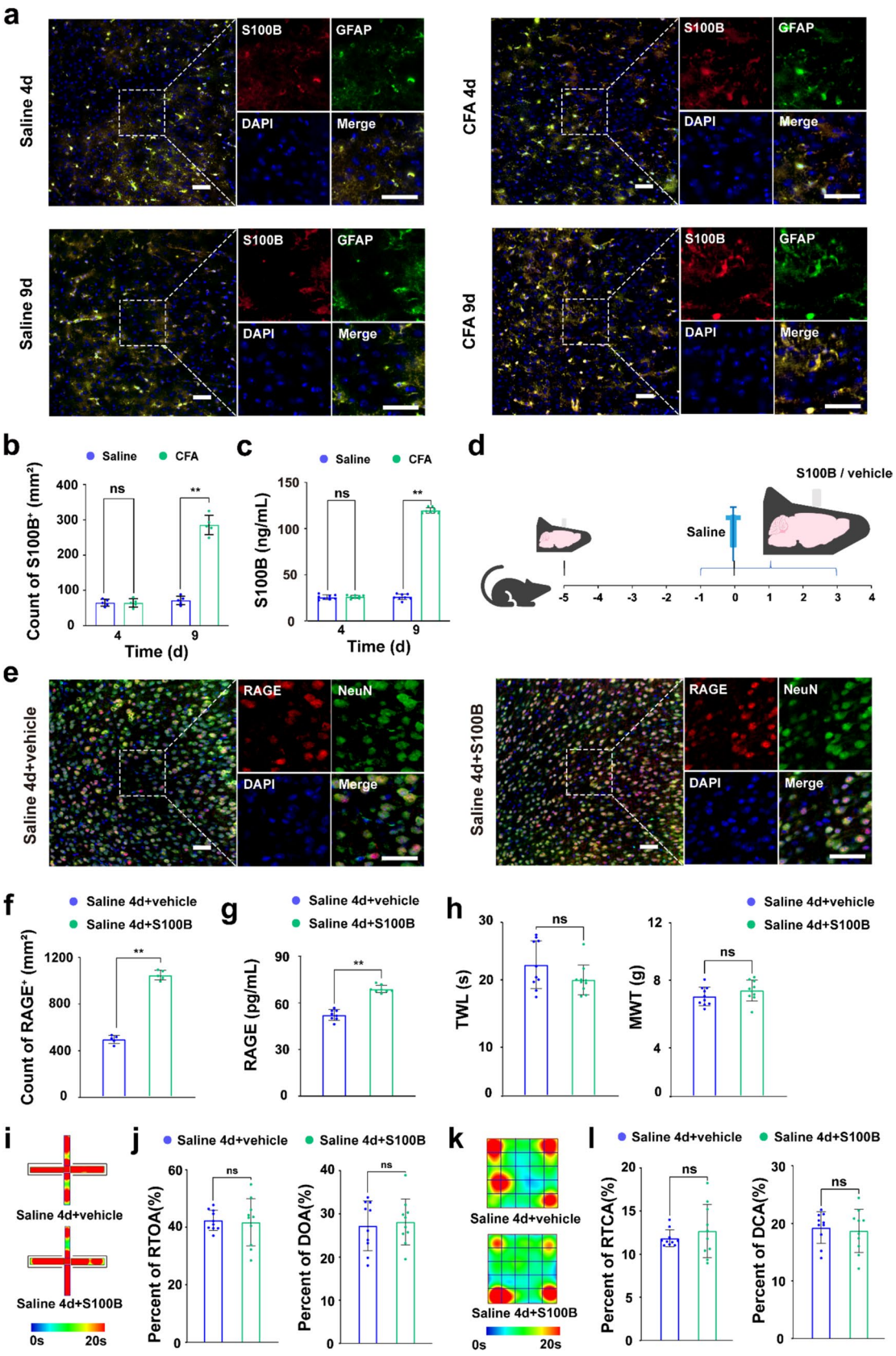
a
Saline 4d
CFA 4d
Saline 9d
CFA 9d
S100B
GFAP
DAPI
Merge
b
Saline
CFA
Count of S100B+ (mm²)
ns
**
Time (d)
c
S100B (ng/mL)
d
S100B / vehicle
Saline
e
Saline 4d+vehicle
Saline 4d+S100B
RAGE
NeuN
f
Count of RAGE+ (mm²)
g
RAGE (pg/mL)
h
TWL (s)
MWT (g)
i
0s
20s
j
Percent of RTOA(%)
Percent of DOA(%)
k
l
Percent of RTCA(%)
Percent of DCA(%)

◂**Fig. 6** S100B was upregulated at 9d after CFA treatment, and intra-ACC injection of S100B activated RAGE but did not induce pain-related behavioral changes under normal conditions. **a**, Immunofluorescence of S100B in ACC astrocytes at different stages after intraplantar CFA or saline injection (scale bar = 50 μm). **b**, Count numbers of S100B-positive cells. **c**, Expression level of S100B in the ACC at different stages after intraplantar CFA or saline injection, as measured by ELISA. **d**, Schematic diagram showing where and when S100B or vehicle was injected into saline-treated mice. **e**, Immunofluorescence of RAGE in the ACC after intra-ACC injection of S100B or vehicle (scale bar = 50 μm). **f**, Count numbers of RAGE-positive cells. **g**, Expression level of RAGE in the ACC after intra-ACC injection of S100B or vehicle, as measured by ELISA. **h**, Thermal withdrawal latency (TWL) and mechanical withdrawal threshold (MWT) of saline-treated mice after S100B or vehicle injection. **i**, Heatmap of saline-treated mice in the elevated plus maze after S100B or vehicle injection (the cross arm of the map is the closed arm, and the longitudinal arm is the open arm). **j**, Calculation of the percentage of time spent in the open arm (RTOA) and the percentage of distance traveled in the open arm (DOA) by the mice in the elevated plus maze. **k**, Heatmap of saline-treated mice in the open field test after S100B or vehicle injection. **l**, Calculation of the percentage of mouse retention time in the central area (RTCA) and the percentage of mouse distance traveled in the central area (DCA) in the open field test.** $p < 0.01$. ns: not significant

Inhibition of RAGE Rescues Hyperexcitability of ACC Neurons at the Late Stage of CIP

Considering that hyperexcitability of ACC neurons plays an important role in inducing a wide range of chronic pain-related behavioral manifestations [2], we aimed to determine whether RAGE modulates ACC neuron excitability in CFA-treated mice.

First, we conducted electrophysiological experiments on day 9 after CFA or saline injection. ACC layer 5 pyramidal neurons were held as the target because of their role in determining the output of the ACC [1]. When holding at resting membrane potential (−65 mV) and a 50 pA depolarizing stimulus were injected, the action potential (AP) number of ACC layer 5 pyramidal neurons was obviously greater in the CFA-treated mice than in the saline-treated mice (one-way ANOVA: $F_{(2,15)} = 17.392$, $p < 0.001$; post hoc Bonferroni correction: Saline 9d vs CFA 9d: $p < 0.001$; Saline 9d $n =$ 6 cells, CFA 9d $n = 6$ cells; Fig. 5a-b). We subsequently assessed the electrophysiology of CFA 9d mice that were pretreated with 5 consecutive days of intra-ACC FPS-ZM1 injection once per day. We found that the AP number of layer 5 pyramidal neurons in the ACC slices obtained at 9 days after CFA injection in CFA 9d+ FPS-ZM1 mice decreased significantly compared with that in CFA 9d mice (post hoc Bonferroni correction: CFA 9d+ FPS-ZM1 vs CFA 9d: $p =$ 0.003) to a level similar to that of the saline group (post hoc Bonferroni correction: CFA 9d+ FPS-ZM1 vs Saline 9d: p = 0.396; CFA 9d+ FPS-ZM1 $n = 6$ cells; Fig. 5b).

Furthermore, we compared the rheobase by administering a series of current steps from 0 to +50 pA in 10 pA increments (Fig. 5c). All the rheobases of neurons in saline-treated 9d mice were larger than or equal to 30 pA, with a median of 40 pA, whereas all the rheobases of neurons in CFA-treated 9d mice were less than or equal to 30 pA, with a median of 15 pA. The median number of rheobases in neurons from CFA 9d+ FPS-ZM1 mice was 35 pA. There was a significant difference between the rheobase grades of the three groups (Kruskal−Wallis H test: $X^2 = 10.311$, $df = 2$, $p = 0.006$; all groups $n = 6$ cells; Fig. 5c−d). More importantly, significant differences existed not only between the Saline 9d group and the CFA 9d group ($X^2 = 7.763$, $df =$ 1, $p = 0.005$) but also between the CFA 9d+FPS-ZM1 group and the CFA 9d group ($X^2 = 6.322$, $df = 1$, $p = 0.012$), indicating that the hyperexcitable state of ACC neurons on day 9 after CFA injection can be reduced by RAGE suppression. These results indicated that RAGE was, at least in part, responsible for the hyperexcitability of ACC neurons at the late stage of CIP.

Upregulation of RAGE in the ACC During CIP Resulted from Activation of Astrocytic S100B

We explored the expression level of S100B in the ACC at days 4 and 9 after intraplantar CFA or saline injection via immunofluorescence and ELISA methods. We found that the S100B-positive cell numbers (one-way ANOVA: $F_{(3,16)} =$ 208.371, $p < 0.001$; post hoc Bonferroni correction: Saline 4d vs CFA 4d: $p = 1.000$, Saline 9d vs CFA 9d: $p < 0.001$; all groups $n = 5$ mice; Fig. 6a-b) and the protein levels of S100B (one-way ANOVA: $F_{(3,28)} = 2564.978$, $p < 0.001$; post hoc Bonferroni correction: Saline 4d vs CFA 4d: $p =$ 1.000, Saline 9d vs CFA 9d: $p < 0.001$; all groups $n = 8$ biological replicates; Fig. 6c) were prominently greater in the CFA group than in the saline group on day 9 but not on day 4, which was consistent with the findings of RAGE expression patterns.

On this basis, we wondered whether intra-ACC injection of S100B could directly increase the expression level of RAGE. First, we conducted 5 days of continuous intra-ACC S100B injection into the mice from 1 day before intraplantar saline injection to 3 days after saline injection. Intra-ACC vehicle injection was used as a control (Fig. 6d). As a result, we found that 5 days of continuous injection of S100B in the ACC of normal mice directly increased the number of RAGE-positive cells (unpaired Student's t test: $t_{(8)} = -22.503$, $p < 0.001$; all groups $n = 5$ mice; Fig. 6e-f) and the protein levels of RAGE in the ACC (unpaired Student's t test: $t_{(14)} = -11.348$, $p < 0.001$; all groups $n = 8$ biological replicates; Fig. 6g). In addition, we also detected the TWL, MWT and anxiety-like behaviors on day 4 after S100B or vehicle injection to determine whether intra-ACC injection of S100B could directly induce chronic pain-related behaviors. Compared with the Saline 4d+vehicle

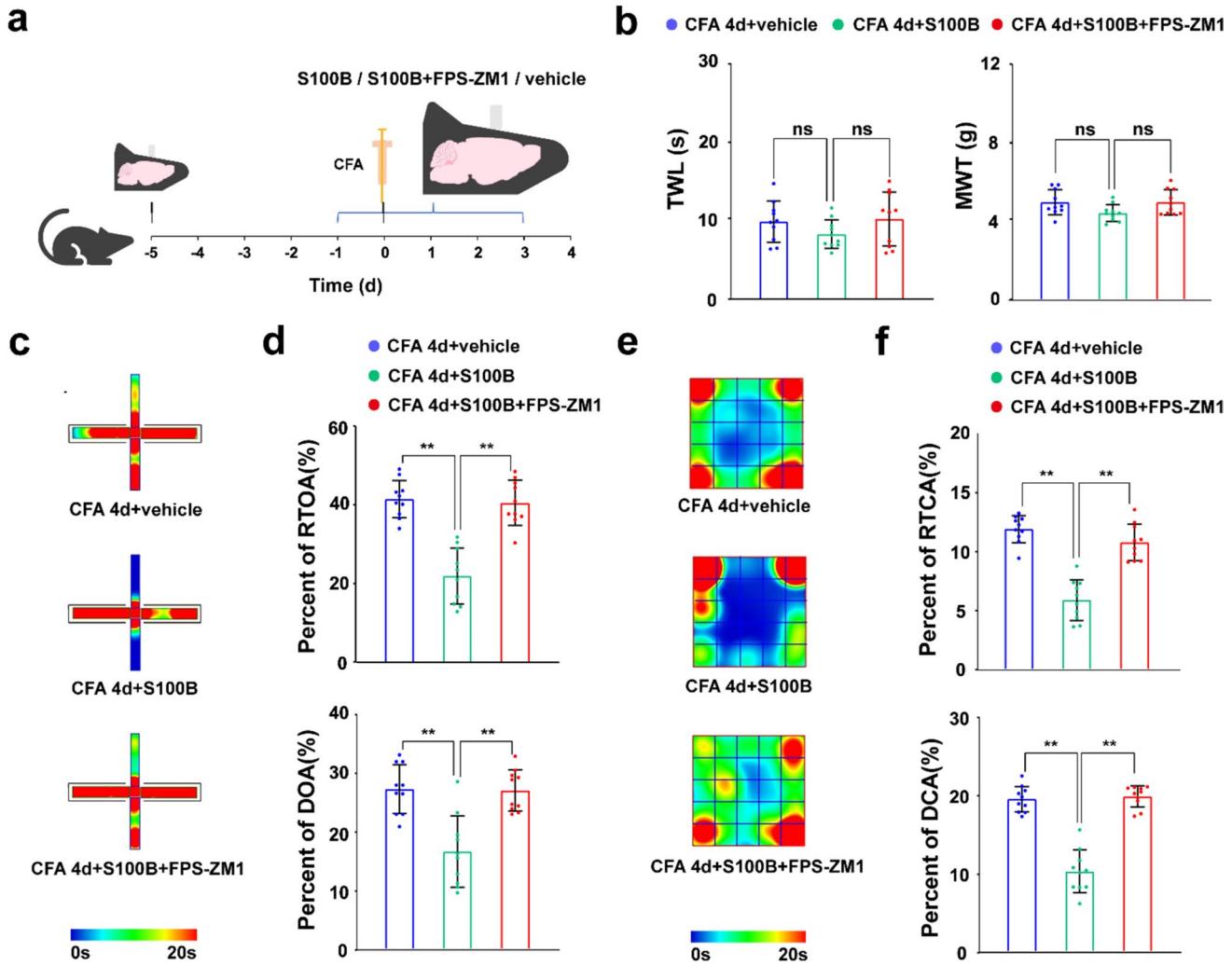

Fig. 7 Activation of RAGE by S100B accelerates the onset of anxiety in CFA-treated mice. **a**, Schematic diagram showing where and when S100B, S100B+FPS-ZM1 or vehicle was injected into CFA-treated mice. **b**, Thermal withdrawal latency (TWL) and mechanical withdrawal threshold (MWT) of CFA-treated mice after S100B, S100B+FPS-ZM1 or vehicle injection. **c**, Heatmap of CFA-treated mice in the elevated plus maze after S100B, S100B+FPS-ZM1 or vehicle injection (the cross arm of the map is the closed arm, and the longitudinal arm is the open arm). **d**, Calculation of the percentage of time spent in the open arm (RTOA) and the percentage of distance traveled in the open arm (DOA) by the mice in the elevated plus maze. **e**, Heatmap of CFA-treated mice in the open field test after S100B, S100B+FPS-ZM1 or vehicle injection. **f**, Calculation of the percentage of mouse retention time in the central area (RTCA) and the percentage of mouse distance traveled in the central area (DCA) in the open field test. ** $p < 0.01$. ns: not significant

mice, the Saline 4d+S100B mice presented similar TWL and MWT (unpaired Student's t test: TWL, $t_{(18)} = 1.688$, $p = 0.109$; MWT, $t_{(18)} = -1.330$, $p = 0.200$; all groups $n = 10$ mice; Fig. 6h). The anxiety-like behaviors of the two groups were also comparable, as reflected by similar RTOA and DOA in the open arms of the elevated plus maze (unpaired Student's t test: RTOA, $t_{(18)} = 0.237$, $p = 0.815$; DOA, $t_{(18)} = -0.353$, $p = 0.728$; all groups $n = 10$ mice; Fig. 6i-j) and similar RTCA and DCA in the central area of the open field (unpaired Student's t test: RTCA, $t_{(18)} = -0.836$, $p = 0.414$; DCA, $t_{(18)} = 0.401$, $p = 0.693$; all groups $n = 10$ mice; Fig. 6k-l). These results indicated that intra-ACC application of S100B alone did not induce pain-related behavioral changes under normal conditions.

Next, we conducted 5 days of continuous ACC-S100B injection from 1 day before intraplantar CFA injection to 3 days after CFA injection and detected behavioral responses on CFA day 4 (Fig. 7a). The results revealed slight downward trends in the TWL and MWT of CFA 4d+S100B mice compared with those of CFA 4d+vehicle mice, but the differences were not statistically significant (CFA 4d+vehicle vs CFA 4d+S100B: TWL, one-way ANOVA: $F_{(2,27)} = 1.449$, $p = 0.252$; post hoc Bonferroni correction: $p = 0.600$; MWT, one-way ANOVA: $F_{(2,27)} = 2.960$, $p =$

0.069; post hoc Bonferroni correction: $p = 0.132$; all groups $n = 10$ mice; Fig. 7b). However, the CFA 4d mice injected with ACC-S100B exhibited much lower levels of RTOA and DOA in the open arm of the elevated plus maze (CFA 4d+vehicle vs. CFA 4d+S100B: RTOA, one-way ANOVA: $F_{(2,27)} = 34.611$, $p < 0.001$; post hoc Bonferroni correction: $p < 0.001$; DOA, one-way ANOVA: $F_{(2,27)} = 16.721$, $p < 0.001$; post hoc Bonferroni correction: $p < 0.001$; all groups $n = 10$ mice; Fig. 7c-d) and much lower levels of RTCA and DCA in the central area of the open field (CFA 4d+vehicle vs. CFA 4d+S100B: RTCA, one-way ANOVA: $F_{(2,27)} = 45.777$, $p < 0.001$; post hoc Bonferroni correction: $p < 0.001$; DCA, one-way ANOVA: $F_{(2,27)} = 72.922$, $p < 0.001$; post hoc Bonferroni correction: $p < 0.001$; all groups $n = 10$ mice; Fig. 7e-f). In addition, we found that injecting 10 mM FPS-ZM1 at the same time as when ACC-S100B was continuously injected into CFA 4d mice slightly but not significantly increased the TWL and MWT (CFA 4d+S100B vs CFA 4d+S100B+FPS-ZM1: TWL, post hoc Bonferroni correction: $p = 0.367$; MWT, post hoc Bonferroni correction: $p = 0.136$; all groups $n = 10$ mice; Fig. 7b) and prevented decreases in the levels of RTOA and DOA in the open arm of the elevated plus maze and RTCA and DCA in the central area of the open field (CFA 4d+S100B vs CFA 4d+S100B+FPS-ZM1: RTOA, post hoc Bonferroni correction: $p < 0.001$; DOA, post hoc Bonferroni correction: $p < 0.001$; RTCA, post hoc Bonferroni correction: $p < 0.001$; DCA, post hoc Bonferroni correction: $p < 0.001$; all groups $n = 10$ mice; Fig. 7c-f). These results indicate that the intra-ACC application of S100B might accelerate the emergence of anxiety in the early stage of inflammatory pain and that this accelerating effect can be blocked by the inhibition of RAGE with FPS-ZM1, suggesting that this effect of S100B is accomplished via the activation of RAGE.

Inhibition of ACC Astrocytic S100B Suppressed RAGE levels and Alleviated Hypersensitivity and Anxiety in CFA-Treated Mice

Next, we suppressed astrocytes via L-α-AA based on previous studies [4, 5] to inhibit the secretion of ACC astrocytic S100B (Fig. 8a). The intra-ACC microinjection of L-α-AA was conducted from day 4 to day 8 after intraplantar CFA injection, such that the protein levels of S100B (unpaired Student's t test: $t_{(14)} = 32.417$, $p < 0.001$; all groups $n = 8$ biological replicates; Fig. 8b) and the number of S100B-positive cells (unpaired Student's t test: $t_{(8)} = 14.336$, $p < 0.001$; all groups $n = 5$ mice; Fig. 8c-d) were significantly reduced. Intra-ACC microinjection of vehicle was used as a control. On day 9 after intraplantar CFA injection, the ELISA and immunofluorescence results confirmed that RAGE protein levels (unpaired Student's t test: $t_{(14)} = 7.669$, $p < 0.001$; all groups $n = 8$ biological replicates) and RAGE-positive neuron numbers (unpaired Student's t test: $t_{(8)} = 7.490$, $p < 0.001$; all groups $n = 5$ mice) were decreased by L-α-AA (Fig. 8e-g), suggesting that ACC astrocytic S100B strongly regulates the upregulation of RAGE.

We also detected causal relationships between astrocytes and behavioral performance in CFA-treated mice on day 9. Our results showed that the CFA-treated mice subjected to intra-ACC L-α-AA injection presented greater TWL and MWT than did those subjected to intra-ACC vehicle injection did (unpaired Student's t test: TWL, $t_{(18)} = -5.818$, $p < 0.001$; MWT, $t_{(18)} = -5.275$, $p < 0.001$; all groups $n = 10$ mice; Fig. 8h), suggesting that hyperalgesia was alleviated by L-α-AA. In the elevated plus-maze test, the CFA-treated mice subjected to intra-ACC L-α-AA injection spent more time and traveled longer distances in the open arms than did the CFA-treated mice subjected to intra-ACC vehicle injection (unpaired Student's t test: RTOA, $t_{(18)} = -4.802$, $p < 0.001$; DOA, $t_{(18)} = -3.918$, $p = 0.001$; all groups $n = 10$ mice; Fig. 8i-j). Similarly, in the open field test, the RTCA and DCA of intra-ACC L-α-AA-injected CFA mice were significantly greater than those of intra-ACC vehicle-injected CFA mice (unpaired Student's t test: RTCA, $t_{(18)} = -3.175$, $p = 0.005$; DCA, $t_{(18)} = -2.435$, $p = 0.026$; all groups $n = 10$ mice; Fig. 8k-l). These results confirmed that suppressing astrocytes alleviated anxiety in CFA-treated mice.

Discussion

Our results revealed that RAGE expression was increased in the ACC at the late stage of inflammatory pain in mice, which was correlated with the maintenance of pain and the comorbidity of anxiety. Inhibition of RAGE activation at the late stage decreased the excitability of ACC neurons and alleviated hyperalgesia and anxiety in CFA-treated mice. Furthermore, we revealed that the increase in RAGE expression might result from the activation of astrocytes in the ACC and the secretion of S100B. Suppression of astrocyte activation also alleviated hyperalgesia and anxiety in CFA-treated mice.

Modulation of RAGE by Astrocytic S100B in CIP

Our elevated plus maze and open field test results revealed that the mice exhibited anxiety-like behavior on the 9th day but not on the 4th day, suggesting that the ACC may exhibit specific neural mechanisms involved in regulating late-phase pain, which is similar to the findings of a previous study [48]. Unlike microglia, which are activated in the acute phases of inflammatory pain, astrocytes participate in the chronic phases of inflammatory pain [6, 49–51]. Neuron−astrocyte coupling facilitates spinal plasticity and the maintenance

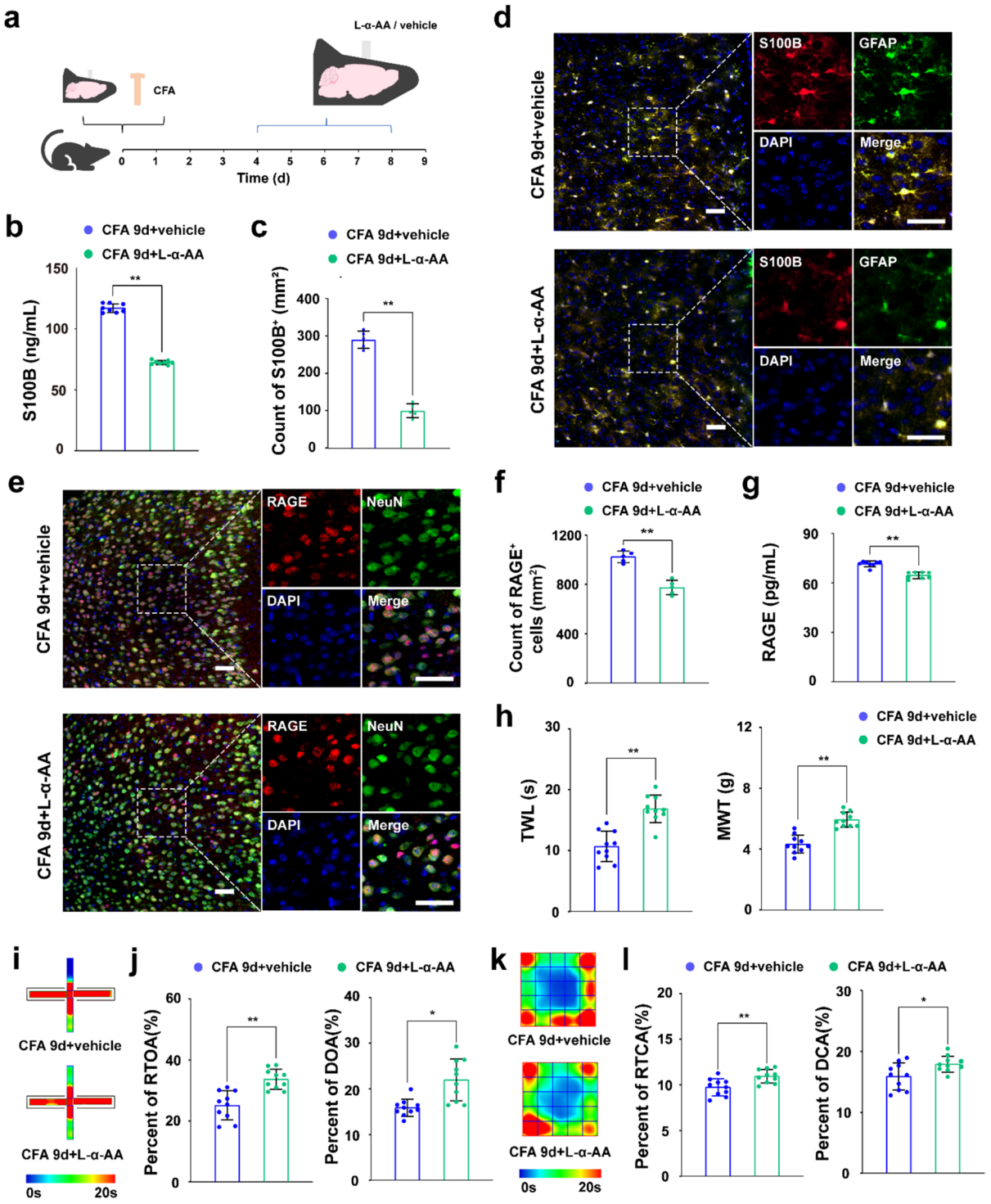

of inflammatory pain, and astrocyte activation in the ACC contributes to comorbid anxiety in the CIP [52, 53], which further emphasizes the importance of astrocytes in the CIP.

S100B can be upregulated in neuroinflammatory conditions and is mainly colocalized with the astrocytic marker GFAP in the cerebral cortex and spinal cord[7]. Therefore, most current studies on S100B in neurological disorders have focused mainly on astrocytes [6, 54–58]. Previous studies have shown that S100B is increased in ACC astrocytes in both CIP and chronic visceral pain rodent models [3–6]. Some of these studies using L-α-AA to suppress astrocytes could downregulate the expression of GFAP and S100B and reduce anxiety and depression-like behavior in the elevated plus maze, forced swimming experiments and

◂**Fig. 8** Intra-ACC injection of L-α-AA reduces RAGE levels and alleviates hypersensitivity and anxiety in CFA-treated mice. **a**, Schematic diagram showing the experimental protocol. **b**, Expression level of S100B in the ACC after L-α-AA or vehicle injection, as measured by ELISA. **c**, Count numbers of S100B-positive neurons. **d**, Immunofluorescence of S100B in ACC astrocytes after L-α-AA or vehicle injection (scale bar = 50 μm). **e**, Immunofluorescence of RAGE in ACC neurons after L-α-AA or vehicle injection (scale bar = 50 μm). **f**, Count numbers of RAGE-positive neurons. **g**, Expression level of RAGE in the ACC after L-α-AA or vehicle injection, as measured by ELISA. **h**, Thermal withdrawal latency (TWL) and mechanical withdrawal threshold (MWT) of CFA-treated mice after L-α-AA or vehicle injection. **i**, Heatmap of CFA-treated mice in the elevated plus maze after L-α-AA or vehicle injection (the cross arm of the map is the closed arm, and the longitudinal arm is the open arm). **j**, Calculation of the percentage of time spent in the open arm (RTOA) and the percentage of distance traveled in the open arm (DOA) by the mice in the elevated plus maze. **k**, Heatmap of CFA-treated mice in the open field test after L-α-AA or vehicle injection. **l**, Calculation of the percentage of mouse retention time in the central area (RTCA) and the percentage of mouse distance traveled in the central area (DCA) in the open field test. * $p < 0.05$, ** $p < 0.01$

avoidance behavior in conditional place avoidance (CPA) [4, 5]. However, whether RAGE, a specific receptor for S100B, is involved in the mechanism of CIP regulation by ACC astrocytic S100B is unclear.

Our study validated the prominent upregulation of S100B and RAGE in the ACC on the 9th day after the establishment of the CIP mouse model and revealed that the expression of RAGE was modulated by intra-ACC S100B injection or inhibition of ACC astrocytes with L-α-AA. These results suggest a causal relationship between S100B and RAGE upregulation in CIP patients, which explains why the upregulation of RAGE in our study occurred in the later stages of CIP, similar to previous findings [59, 60]. Therefore, these findings indicate that RAGE may play a role in mediating the effect of S100B in the late phase of pain.

Cortical RAGE and Pathological Pain

In recent years, RAGE has been found to be present on the neurocytic membrane of the DRG [12, 22] and SDH [13, 14, 61]. Although RAGE is not expressed only in neurons, all of these previous studies on the role of RAGE in pain regulation focused mainly on neurons and confirmed that RAGE on the DRG and SDH neuronal membrane participates in the pathogenesis of pathological pain [12, 18, 23, 24, 62–64]. Intraperitoneal or intrathecal injection of RAGE inhibitors, including low-molecular-weight heparin [19, 22, 24, 65], papaverine [60], FPS-ZM1 [12, 22, 24, 66], monoclonal antibody against RAGE [59], or anti-RAGE neutralizing antibodies [13, 64, 67], inhibits the upregulation of RAGE expression in the DRG and SDH, which can relieve or even prevent the pain sensitivity of experimental animals. In vitro studies have shown that when RAGE expression is upregulated on the SDH neuronal membrane, it can significantly increase the miniature excitatory postsynaptic currents (mEPSC) of SDH neurons, causing long-term potentiation (LTP) of C-fiber-evoked potentials, leading to central sensitization [13]. When RAGE is activated in DRG neurons, it has a mutual effect with the transient receptor potential vanilloid-1 (TRPV1) channel, leading to peripheral sensitization [12]. However, it is unclear whether supraspinal RAGEs are involved in pain regulation.

The ACC is an important center for nociceptive sensation [1, 2]. Our results revealed that RAGE was expressed on the PAG-projecting ACC neuronal membrane. Given the pivotal role of the ACC−PAG pathway in modulating pain thresholds [46], it is reasonable to believe that RAGE in the ACC may influence pain thresholds. FPS-ZM1 is a RAGE-specific inhibitor that can competitively inhibit RAGE activation [40]. Previous studies have shown that continuous administration of FPS-ZM1 prevents the increase in RAGE expression levels. This effect may be related to the inhibition of the positive feedback of RAGE transcription via the inhibition of its downstream pathway [22, 24, 66, 68–70]. Accordingly, we downregulated RAGE via repeated administration of FPS-ZM1 in the ACC and showed that FPS-ZM1 strongly alleviated pain-related hypersensitivity and reduced hyperexcitability of ACC layer 5 pyramidal neurons at the late stage. The possibility that other neuron types within the ACC are affected by CFA treatment and FPS-ZM1 has not been explored, which is a limitation of our study.

In contrast, previous studies have shown that intra-ACC microinjection of L-α-AA cannot alleviate mechanical allodynia in mouse pain models [4, 5]. The major difference is that those studies only treated the mice once and conducted behavioral tests in the short term; as a result, it was not sufficient to affect the expression level of RAGE or the pain threshold values. In the present study, we administered L-α-AA for 5 days to persistently block the upregulation of RAGE expression induced by S100B, which significantly alleviated mechanical allodynia in CFA-treated mice. These results indicate that RAGE in the ACC may play an important role in the maintenance of pain perception.

Role of RAGE in Anxiety Comorbidity

There is some evidence indicating that the expression of RAGE is upregulated in the central nervous system of patients with psychiatric disorders such as delirium [29], schizophrenia [25–27] and depression [28]. Inhibiting the upregulation of RAGE in the prefrontal cortex via the use of FPS-ZM1 or knocking out the RAGE gene prevented or alleviated depressive behavior in rodent models [71, 72]. However, it is unclear whether RAGE directly participates in the regulation of anxiety in chronic pain conditions.

In fact, the timing of anxiety-like behavior in CFA-induced inflammatory pain mouse models has varied in

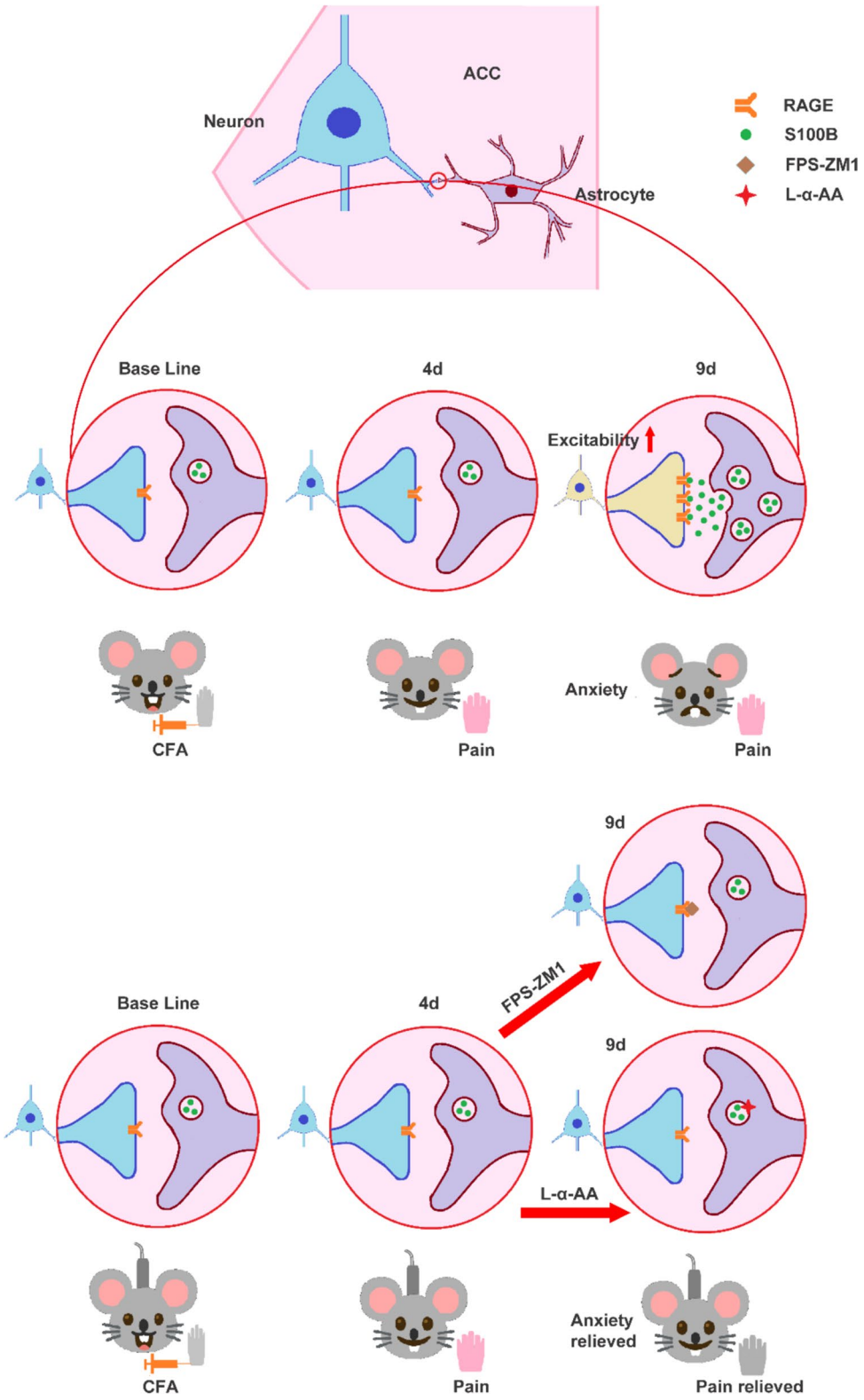

Fig. 9 Graphical abstract of the experimental design

previous studies, which may be influenced by the source of the mice, the experimental manipulations, and the experimental environment. Our present results revealed that anxiety mainly occurs on day 9 after intraplantar CFA injection and that direct downregulation of RAGE expression in the ACC significantly alleviated anxiety-like behavior in CFA-treated mice. The ACC is an important center for the processing of pain-related emotion [2], and

our and other reports have confirmed the role of the ACC-VTA in modulating chronic pain comorbid with emotional symptoms [41, 47], such as aversion and anxiety. Here, we showed that most VTA-projecting ACC neurons exhibit RAGE, which provides an anatomic basis for the ability of RAGE to regulate chronic pain comorbid with anxiety. The upregulation of S100B and RAGE in the ACC occurred at the same time as the onset of anxiety-like behavior in mice, suggesting that the activation of RAGE by ACC astrocytic S100B may be a key factor in the development of anxiety in the later stages of CIP. Interestingly, although the upregulation of RAGE by S100B did not induce obvious hypersensitivity or anxiety in normal mice, it slightly aggravated the development of hyperalgesia and induced anxiety in the early phase of CIP on the 4th day after CFA injection, which could be reversed by injecting FPS-ZM1 at the same time. These results indicate that RAGE in the ACC may play an important role in facilitating the development of hyperalgesia and anxiety in CIP patients.

A wide variety of evidence has demonstrated that pain and negative affect are anatomically and functionally integrated in the dorsal ACC (dACC) [73].Therefore, this study primarily analyzed the fluorescence signals in the dACC area, and the possibility of whether neurons within other areas of the ACC are affected by CFA treatment and FPS-ZM1 has not been explored. There were several limitations in our study. First, a previous study revealed that HMGB1 was increased in the ACC of inflammatory pain model mice but was not associated with emotional response changes [74]. However, the crosstalk between HMGB1 and RAGE in regulating pain behaviors still needs to be further investigated. Second, we did not explore the role of S100B and RAGE in other cell types, which is also an important issue for future studies. Next, not setting more elaborate time points for detecting RAGE levels to draw an expression curve and better show the changing process of RAGE expression levels is a shortcoming of this study. In addition, it should be acknowledged that the lack of further exploration of the role of estrogen in chronic inflammatory pain is a limitation of our study.

Conclusions

In conclusion, we provide direct evidence that RAGE in ACC neurons plays an important role in astrocytic regulation of CIP and anxiety comorbidity in CIP mice. ACC neuronal RAGE upregulation results from the activation of astrocytic S100B and leads to the maintenance of pain perception and anxiety in the late phase after CFA injection. Direct inhibition of RAGE in the ACC is an important way to alleviate both hyperalgesia and anxiety in the late phase after CFA injection (Fig. 9). These findings, at least in part, explain the mechanism by which ACC neuron−astrocyte coupling promotes the maintenance of inflammatory pain and anxiety comorbidity and provide new therapeutic avenues for the treatment of CIP and anxiety comorbidity.

Supplementary Information The online version contains supplementary material available at https://doi.org/10.1007/s12035-025-04713-y.

Author Contributions W.J., P.C., S.G. and Z.X. primarily conceived the work; L.S. and C.Y. investigated the background; W.J., P.C., S.G. and M.G. collected the data; W.J. and S.G. analyzed the data; W.J. and S.G. wrote the manuscript and prepared the figures; Z.X., P.C. and H.R. reviewed and edited the manuscript. All authors reviewed the manuscript.

Funding This work was supported by the Basic Research Program of Science and Technology Department of Guizhou Province (Grant numbers [ZK[2024]yiban266]); the Natural Science Foundation of Chongqing Municipality (Grant numbers [CSTB2023NSCQ-MSX0009]); the National Natural Science Foundation of China (Grant numbers [81760214] and [81971059]); and the Project of Key Laboratory of Anesthesia and Organ Protection, Zunyi Medical University (Grant numbers [Qianjiaoji[2023]106]).

Data Availability No datasets were generated or analysed during the current study.

Declarations

Ethics Approval All animal experiments were approved by the animal experiment ethics committee of Zunyi Medical University (ZMU21-2306-024). Animal studies were carried out in accordance with the National Research Council (NIH) Guide for the Care and Use of Laboratory Animals and complied with relevant sections of the Animal Research: Reporting of In Vivo Experiments (ARRIVE) guidelines.

Competing Interests The authors declare no competing interests.

References

1. Gao SH, Shen LL, Wen HZ, Zhao YD, Ruan HZ (2017) Inhibition of Metabotropic glutamate receptor subtype 1 alters the excitability of the commissural pyramidal neuron in the rat anterior cingulate cortex after chronic constriction injury to

the sciatic nerve. Anesthesiology 127:515–33. https://doi.org/10.1097/ALN.0000000000001654
2. Bliss TV, Collingridge GL, Kaang BK, Zhuo M (2016) Synaptic plasticity in the anterior cingulate cortex in acute and chronic pain. Nat Rev Neurosci 17:485–96. https://doi.org/10.1038/nrn.2016.68
3. Lu Y, Zhu L, Gao YJ (2011) Pain-related aversion induces astrocytic reaction and proinflammatory cytokine expression in the anterior cingulate cortex in rats. Brain Res Bull 84:178–82. https://doi.org/10.1016/j.brainresbull.2010.12.007
4. Ikeda H, Mochizuki K, Murase K (2013) Astrocytes are involved in long-term facilitation of neuronal excitation in the anterior cingulate cortex of mice with inflammatory pain. Pain 154:2836–43. https://doi.org/10.1016/j.pain.2013.08.023
5. Chen FL, Dong YL, Zhang ZJ, Cao DL, Xu J, Hui J et al (2012) Activation of astrocytes in the anterior cingulate cortex contributes to the affective component of pain in an inflammatory pain model. Brain Res Bull 87:60–6. https://doi.org/10.1016/j.brainresbull.2011.09.022
6. Wang J, Tu J, Cao B, Mu L, Yang X, Cong M et al (2017) Astrocytic l-Lactate signaling facilitates amygdala-anterior cingulate cortex synchrony and decision making in rats. Cell Rep 21:2407–18. https://doi.org/10.1016/j.celrep.2017.11.012
7. Michetti F, Di Sante G, Clementi ME, Sampaolese B, Casalbore P, Volonté C et al (2021) Growing role of S100B protein as a putative therapeutic target for neurological- and nonneurological-disorders. Neurosci Biobehav Rev 127:446–58. https://doi.org/10.1016/j.neubiorev.2021.04.035
8. Nishiyama H, Knopfel T, Endo S, Itohara S (2002) Glial protein S100B modulates long-term neuronal synaptic plasticity. Proc Natl Acad Sci U S A 99:4037–42. https://doi.org/10.1073/pnas.052020999
9. Kato J, Agalave NM, Svensson CI (2016) Pattern recognition receptors in chronic pain: mechanisms and therapeutic implications. Eur J Pharmacol 788:261–73. https://doi.org/10.1016/j.ejphar.2016.06.039
10. Araldi D, Khomula EV, Bonet IJM, Bogen O, Green PG, Levine JD (2024) Role of pattern recognition receptors in chemotherapy-induced neuropathic pain. Brain 147:1025–42. https://doi.org/10.1093/brain/awad339
11. Yadav S, Surolia A (2019) Lysozyme elicits pain during nerve injury by neuronal Toll-like receptor 4 activation and has therapeutic potential in neuropathic pain. Sci Transl Med 11. https://doi.org/10.1126/scitranslmed.aav4176
12. Bestall SM, Hulse RP, Blackley Z, Swift M, Ved N, Paton K et al (2018) Sensory neuronal sensitisation occurs through HMGB-1-RAGE and TRPV1 in high-glucose conditions. J Cell Sci 131. https://doi.org/10.1242/jcs.215939
13. Wei JY, Liu CC, Ouyang HD, Ma C, Xie MX, Liu M et al (2017) Activation of RAGE/STAT3 pathway by methylglyoxal contributes to spinal central sensitization and persistent pain induced by bortezomib. Exp Neurol 296:74–82. https://doi.org/10.1016/j.expneurol.2017.07.010
14. Zhang X, Xu L, Chen W, Yu X, Shen L, Huang Y (2020) Pyridoxamine alleviates mechanical allodynia by suppressing the spinal receptor for advanced glycation end product-nuclear factor-κB/extracellular signal-regulated kinase signaling pathway in diabetic rats. Mol Pain 16:1744806920917251. https://doi.org/10.1177/1744806920917251
15. Villarreal A, Seoane R, González Torres A, Rosciszewski G, Angelo MF, Rossi A et al (2014) S100B protein activates a RAGE-dependent autocrine loop in astrocytes: implications for its role in the propagation of reactive gliosis. J Neurochem 131:190–205. https://doi.org/10.1111/jnc.12790
16. Schmitt KR, Kern C, Lange PE, Berger F, Abdul-Khaliq H, Hendrix S (2007) S100B modulates IL-6 release and cytotoxicity from hypothermic brain cells and inhibits hypothermia-induced axonal outgrowth. Neurosci Res 59:68–73. https://doi.org/10.1016/j.neures.2007.05.011
17. Ponath G, Schettler C, Kaestner F, Voigt B, Wentker D, Arolt V et al (2007) Autocrine S100B effects on astrocytes are mediated via RAGE. J Neuroimmunol 184:214–22. https://doi.org/10.1016/j.jneuroim.2006.12.011
18. Bufalo MC, Almeida ME, Franca IA, Zambelli VO, Martins Sant'anna MB, Kimura LF et al (2019) Advanced glycation endproducts produced by in vitro glycation of type I collagen modulate the functional and secretory behavior of dorsal root ganglion cells cultivated in two-dimensional system. Exp Cell Res 382:111475. https://doi.org/10.1016/j.yexcr.2019.06.020
19. Matsuura W, Harada S, Liu K, Nishibori M, Tokuyama S (2018) Evidence of a role for spinal HMGB1 in ischemic stress-induced mechanical allodynia in mice. Brain Res 1687:1–10. https://doi.org/10.1016/j.brainres.2018.02.026
20. Kato J, Svensson CI (2015) Role of extracellular damage-associated molecular pattern molecules (DAMPs) as mediators of persistent pain. Prog Mol Biol Transl Sci 131:251–79. https://doi.org/10.1016/bs.pmbts.2014.11.014
21. An K, Rong H, Ni H, Zhu C, Xu L, Liu Q et al (2018) Spinal PKC activation - induced neuronal HMGB1 translocation contributes to hyperalgesia in a bone cancer pain model in rats. Exp Neurol 303:80–94. https://doi.org/10.1016/j.expneurol.2018.02.003
22. Sekiguchi F, Domoto R, Nakashima K, Yamasoba D, Yamanishi H, Tsubota M et al (2018) Paclitaxel-induced HMGB1 release from macrophages and its implication for peripheral neuropathy in mice: Evidence for a neuroimmune crosstalk. Neuropharmacology 141:201–13. https://doi.org/10.1016/j.neuropharm.2018.08.040
23. Nishida T, Tsubota M, Kawaishi Y, Yamanishi H, Kamitani N, Sekiguchi F et al (2016) Involvement of high mobility group box 1 in the development and maintenance of chemotherapy-induced peripheral neuropathy in rats. Toxicology 365:48–58. https://doi.org/10.1016/j.tox.2016.07.016
24. Tsubota M, Fukuda R, Hayashi Y, Miyazaki T, Ueda S, Yamashita R et al (2019) Role of non-macrophage cell-derived HMGB1 in oxaliplatin-induced peripheral neuropathy and its prevention by the thrombin/thrombomodulin system in rodents: negative impact of anticoagulants. J Neuroinflammation 16:199. https://doi.org/10.1186/s12974-019-1581-6
25. Dwir D, Giangreco B, Xin L, Tenenbaum L, Cabungcal JH, Steullet P et al (2020) MMP9/RAGE pathway overactivation mediates redox dysregulation and neuroinflammation, leading to inhibitory/excitatory imbalance: a reverse translation study in schizophrenia patients. Mol Psychiatry 25:2889–904. https://doi.org/10.1038/s41380-019-0393-5
26. Kouidrat Y, Amad A, Desailloud R, Diouf M, Fertout E, Scoury D et al (2013) Increased advanced glycation end-products (AGEs) assessed by skin autofluorescence in schizophrenia. J Psychiatr Res 47:1044–8. https://doi.org/10.1016/j.jpsychires.2013.03.016
27. Kouidrat Y, Amad A, Arai M, Miyashita M, Lalau JD, Loas G et al (2015) Advanced glycation end products and schizophrenia: a systematic review. J Psychiatr Res 66–67:112–7. https://doi.org/10.1016/j.jpsychires.2015.04.023
28. Li J, Zeng Q, Su W, Song M, Xie M, Mao L (2021) FBXO10 prevents chronic unpredictable stress-induced behavioral despair and cognitive impairment through promoting RAGE degradation. CNS Neurosci Ther 27:1504–17. https://doi.org/10.1111/cns.13727
29. Kaźmierski J, Miler P, Pawlak A, Jerczyńska H, Woźniak J, Frankowska E et al (2021) Oxidative stress and soluble receptor for advanced glycation end-products play a role in the pathophysiology of delirium after cardiac surgery. Sci Rep 11:23646. https://doi.org/10.1038/s41598-021-03007-2
30. Zhu X, Tang HD, Dong WY, Kang F, Liu A, Mao Y et al (2021) Distinct thalamocortical circuits underlie allodynia induced by

tissue injury and by depression-like states. Nat Neurosci 24:542–53. https://doi.org/10.1038/s41593-021-00811-x
31. Pitzer C, La Porta C, Treede R-D, Tappe-Theodor A (2019) Inflammatory and neuropathic pain conditions do not primarily evoke anxiety-like behaviours in C57BL/6 mice. Eur J Pain 23:285–306. https://doi.org/10.1002/ejp.1303
32. Labonté B, Engmann O, Purushothaman I, Menard C, Wang J, Tan C et al (2017) Sex-specific transcriptional signatures in human depression. Nat Med 23:1102–11. https://doi.org/10.1038/nm.4386
33 Stoyanova M, Hope DA (2012) Gender, gender roles, and anxiety: Perceived confirmability of self report, behavioral avoidance, and physiological reactivity. J Anxiety Disord 26:206–14. https://doi.org/10.1016/j.janxdis.2011.11.006
34. Van Der Lee S, Boot LM (1955) Spontaneous pseudopregnancy in mice. Acta Physiol Pharmacol Neerl 4:442–4
35. Corder G, Doolen S, Donahue RR, Winter MK, Jutras BL, He Y et al (2013) Constitutive μ-opioid receptor activity leads to long-term endogenous analgesia and dependence. Science 341:1394–9. https://doi.org/10.1126/science.1239403
36. Scheff NN, Gold MS (2015) Trafficking of Na+/Ca2+ exchanger to the site of persistent inflammation in nociceptive afferents. J Neurosci 35:8423–32. https://doi.org/10.1523/JNEUROSCI.3597-14.2015
37. Costa MDC, Sutter PD, Gybels J, Hees JV (1981) Adjuvant-induced arthritis in rats: a possible animal model of chronic pain. Pain 10:173–85. https://doi.org/10.1016/0304-3959(81)90193-7
38. Pan Z, Zhu LJ, Li YQ, Hao LY, Yin C, Yang JX et al (2014) Epigenetic modification of spinal miR-219 expression regulates chronic inflammation pain by targeting CaMKIIgamma. J Neurosci 34:9476–83. https://doi.org/10.1523/JNEUROSCI.5346-13.2014
39. Paxinos G, Franklin KBJ (2012) Paxinos and Franklin's the mouse brain in stereotaxic coordinates. Academic Press of Elsevier, New York
40. Deane R, Singh I, Sagare AP, Bell RD, Ross NT, LaRue B et al (2012) A multimodal RAGE-specific inhibitor reduces amyloid β-mediated brain disorder in a mouse model of Alzheimer disease. J Clin Invest 122:1377–92. https://doi.org/10.1172/jci58642
41. Gao S-H, Shen L-L, Wen H-Z, Zhao Y-D, Chen P-H, Ruan H-Z (2020) The projections from the anterior cingulate cortex to the nucleus accumbens and ventral tegmental area contribute to neuropathic pain-evoked aversion in rats. Neurobiol Dis 140:104862. https://doi.org/10.1016/j.nbd.2020.104862
42. Yokoi K, Kachi S, Zhang HS, Gregory PD, Spratt SK, Samulski RJ et al (2007) Ocular gene transfer with self-complementary AAV vectors. Invest Ophthalmol Vis Sci 48:3324–8. https://doi.org/10.1167/iovs.06-1306
43. Marcantoni A, Raymond EF, Carbone E, Marie H (2013) Firing properties of entorhinal cortex neurons and early alterations in an Alzheimer's disease transgenic model. Pflugers Arch 466:1437–50. https://doi.org/10.1007/s00424-013-1368-z
44. Wang H, Westin L, Nong Y, Birnbaum S, Bendor J, Brismar H et al (2009) Norbin is an endogenous regulator of metabotropic glutamate receptor 5 signaling. Science 326:1554–7. https://doi.org/10.1126/science.1178496
45. Tao C, Zhang G-W, Huang JJ, Li Z, Tao HW, Zhang LI (2023) The medial preoptic area mediates depressive-like behaviors induced by ovarian hormone withdrawal through distinct GABAergic projections. Nat Neurosci 26:1529–40. https://doi.org/10.1038/s41593-023-01397-2
46. Lee JY, You T, Lee CH, Im GH, Seo H, Woo CW et al (2022) Role of anterior cingulate cortex inputs to periaqueductal gray for pain avoidance. Curr Biol 32:2834–47.e5. https://doi.org/10.1016/j.cub.2022.04.090
47. Song Q, Wei A, Xu H, Gu Y, Jiang Y, Dong N et al (2024) An ACC-VTA-ACC positive-feedback loop mediates the persistence of neuropathic pain and emotional consequences. Nat Neurosci 27:272–85. https://doi.org/10.1038/s41593-023-01519-w
48. Morales-Medina JC, Bautista-Carro MA, Serrano-Bello G, Sánchez-Teoyotl P, Vásquez-Ramírez AG, Iannitti T (2023) Persistent peripheral inflammation and pain induces immediate early gene activation in supraspinal nuclei in rats. Behav Brain Res 446:114395. https://doi.org/10.1016/j.bbr.2023.114395
49. Raghavendra V, Tanga FY, DeLeo JA (2004) Complete Freunds adjuvant-induced peripheral inflammation evokes glial activation and proinflammatory cytokine expression in the CNS. Eur J Neurosci 20:467–73. https://doi.org/10.1111/j.1460-9568.2004.03514.x
50. Hansen RR, Malcangio M (2013) Astrocytes–multitaskers in chronic pain. Eur J Pharmacol 716:120–8. https://doi.org/10.1016/j.ejphar.2013.03.023
51. Deng GC, Lu M, Zhao YY, Yuan Y, Chen G (2019) Activated spinal astrocytes contribute to the later phase of carrageenan-induced prostatitis pain. J Neuroinflammation 16:189. https://doi.org/10.1186/s12974-019-1584-3
52. Marty-Lombardi S, Lu S, Ambroziak W, Schrenk-Siemens K, Wang J, DePaoli-Roach AA et al (2024) Neuron-astrocyte metabolic coupling facilitates spinal plasticity and maintenance of inflammatory pain. Nat Metab. https://doi.org/10.1038/s42255-024-01001-2
53. Wei N, Guo Z, Qiu M, Ye R, Shao X, Liang Y et al (2024) Astrocyte activation in the ACC contributes to comorbid anxiety in chronic inflammatory pain and involves in the excitation-inhibition imbalance. Mol Neurobiol. https://doi.org/10.1007/s12035-024-04027-5
54. Langeh U, Singh S (2021) Targeting S100B Protein as a Surrogate Biomarker and its Role in Various Neurological Disorders. Curr Neuropharmacol 19:265–77. https://doi.org/10.2174/1570159x18666200729100427
55. Pan M, Roe JM, Nudel R, Schork AJ, Iakunchykova O, Fjell AM et al (2023) Circulating S100B levels at birth and risk of six major neuropsychiatric or neurological disorders: a two-sample Mendelian Randomization Study. Transl Psychiatry 13:174. https://doi.org/10.1038/s41398-023-02478-3
56. Hughes CG, Patel MB, Brummel NE, Thompson JL, McNeil JB, Pandharipande PP et al (2018) Relationships between markers of neurologic and endothelial injury during critical illness and long-term cognitive impairment and disability. Intensive Care Med 44:345–55. https://doi.org/10.1007/s00134-018-5120-1
57. Yelmo-Cruz S, Morera-Fumero AL, Abreu-González P (2013) S100B and schizophrenia. Psychiatry Clin Neurosci 67:67–75. https://doi.org/10.1111/pcn.12024
58. Bjursten S, Pandita A, Zhao Z, Fröjd C, Ny L, Jensen C et al (2021) Early rise in brain damage markers and high ICOS expression in CD4+ and CD8+ T cells during checkpoint inhibitor-induced encephalomyelitis. J Immunother Cancer 9. https://doi.org/10.1136/jitc-2021-002732
59. Allette YM, Due MR, Wilson SM, Feldman P, Ripsch MS, Khanna R et al (2014) Identification of a functional interaction of HMGB1 with Receptor for Advanced Glycation End-products in a model of neuropathic pain. Brain Behav Immun 42:169–77. https://doi.org/10.1016/j.bbi.2014.06.199
60. Yoshizawa K, Takeuchi K, Nakamura T, Ukai S, Takahashi Y, Sato A et al (2021) Antinociceptive activity of the novel RAGE inhibitor, papaverine, in a mouse model of chronic inflammatory pain. Synapse 75:e22188. https://doi.org/10.1002/syn.22188
61. Qian J, Zhu Y, Bai L, Gao Y, Jiang M, Xing F et al (2020) Chronic morphine-mediated upregulation of high mobility group box 1 in the spinal cord contributes to analgesic tolerance and hyperalgesia in rats. Neurotherapeutics 17:722–42. https://doi.org/10.1007/s13311-019-00800-w
62. Tsujita R, Tsubota M, Hayashi Y, Saeki H, Sekiguchi F, Kawabata A (2018) Role of Thrombin in Soluble Thrombomodulin-Induced Suppression of Peripheral HMGB1-Mediated Allodynia in Mice.

J Neuroimmune Pharmacol 13:179–88. https://doi.org/10.1007/s11481-017-9773-2
63. Tsujita R, Tsubota M, Sekiguchi F, Kawabata A (2021) Role of high-mobility group box 1 and its modulation by thrombomodulin/thrombin axis in neuropathic and inflammatory pain. Br J Pharmacol 178:798–812. https://doi.org/10.1111/bph.15091
64 Liao HY, Hsieh CL, Huang CP, Lin YW (2017) Electroacupuncture attenuates cfa-induced inflammatory pain by suppressing Nav1.8 through S100B, TRPV1, opioid, and adenosine pathways in mice. Sci Rep 7:42531. https://doi.org/10.1038/srep42531
65. Tomita S, Sekiguchi F, Kasanami Y, Naoe K, Tsubota M, Wake H et al (2020) Ca(v)3.2 overexpression in L4 dorsal root ganglion neurons after L5 spinal nerve cutting involves Egr-1, USP5 and HMGB1 in rats: an emerging signaling pathway for neuropathic pain. Eur J Pharmacol 888:173587. https://doi.org/10.1016/j.ejphar.2020.173587
66. Zhang XS, Li X, Luo HJ, Huang ZX, Liu CC, Wan Q et al (2017) Activation of the RAGE/STAT3 pathway in the dorsal root ganglion contributes to the persistent pain hypersensitivity induced by lumbar disc herniation. Pain Phys 20:419–27
67. Li X, Yang H, Ouyang Q, Liu F, Li J, Xiang Z et al (2016) Enhanced RAGE expression in the dorsal root ganglion may contribute to neuropathic pain induced by spinal nerve ligation in rats. Pain Med 17:803–12. https://doi.org/10.1093/pm/pnv035
68. Xie J, Méndez JD, Méndez-Valenzuela V, Aguilar-Hernández MM (2013) Cellular signalling of the receptor for advanced glycation end products (RAGE). Cell Signal 25:2185–97. https://doi.org/10.1016/j.cellsig.2013.06.013
69. Ott C, Jacobs K, Haucke E, Navarrete Santos A, Grune T, Simm A (2014) Role of advanced glycation end products in cellular signaling. Redox Biol 2:411–29. https://doi.org/10.1016/j.redox.2013.12.016
70. Hudson BI, Lippman ME (2018) Targeting RAGE signaling in inflammatory disease. Annu Rev Med 69:349–64. https://doi.org/10.1146/annurev-med-041316-085215
71. Franklin TC, Wohleb ES, Zhang Y, Fogaça M, Hare B, Duman RS (2018) Persistent increase in microglial RAGE contributes to chronic stress-induced priming of depressive-like behavior. Biol Psychiatry 83:50–60. https://doi.org/10.1016/j.biopsych.2017.06.034
72. Ergenc M, Ozacmak HS, Turan I, Ozacmak VH (2022) Melatonin reverses depressive and anxiety like-behaviours induced by diabetes: involvement of oxidative stress, age, rage and S100B levels in the hippocampus and prefrontal cortex of rats. Arch Physiol Biochem 128:402–10. https://doi.org/10.1080/13813455.2019.1684954
73. Shackman AJ, Salomons TV, Slagter HA, Fox AS, Winter JJ, Davidson RJ (2011) The integration of negative affect, pain and cognitive control in the cingulate cortex. Nat Rev Neurosci 12:154–67. https://doi.org/10.1038/nrn2994
74. Qiu C, Yang LD, Yu W, Tian DD, Gao MR, Wang WJ et al (2021) Paeonol ameliorates CFA-induced inflammatory pain by inhibiting HMGB1/TLR4/NF-κB p65 pathway. Metab Brain Dis 36:273–83. https://doi.org/10.1007/s11011-020-00645-9

Authors and Affiliations

Wei Jiang[1,2] · Minmin Gong[3,4] · Linlin Shen[5] · Chenghui Yu[6] · Huaizhen Ruan[7] · Penghui Chen[7] · Shihao Gao[2] · Zhi Xiao[8,9]

✉ Penghui Chen
chenpenghui@tmmu.edu.cn

✉ Shihao Gao
gshll@tmmu.edu.com

✉ Zhi Xiao
zhixiao@zmu.edu.cn

Wei Jiang
isunsang@tmmu.edu.cn

Minmin Gong
2755304009@qq.com

Linlin Shen
shlldyx@163.com

Chenghui Yu
chenghuiyu@ctbu.edu.cn

Huaizhen Ruan
hzruan163@163.com

[1] Key Laboratory of Anesthesia and Organ Protection (Zunyi Medical University), Ministry of Education, Zunyi Medical University, Xinpu New District Campus No. 1 Street, Zunyi 563000, Guizhou, China

[2] Department of Rehabilitation Medicine, Daping Hospital, Army Medical University, No. 10 Changjiang branch Road, Chongqing 400042, China

[3] Graduate School, Zunyi Medical University, Xinpu New District Campus No. 1 Street, Zunyi 563000, Guizhou, China

[4] Department of Physiology, School of Preclinical Medicine Science, Zunyi Medical University, Xinpu New District Campus No. 1 Street, Zunyi 563000, Guizhou, China

[5] Department of Respiratory and Critical Care Medicine, Xinqiao Hospital, Army Medical University, No. 83 Xinqiao Street, Chongqing 400037, China

[6] Chongqing Key Laboratory of Micro-Nano Systems and Intelligent Transduction, Chongqing Technology and Business University, Eshibaoshan, Chongqing 400067, China

[7] Department of Neurobiology, College of Basic Medical Science, Chongqing Key Laboratory of Neurobiology, Army Medical University, No. 30 Gaotanyan Street, Chongqing 400038, China

[8] Guizhou Key Laboratory of Brain Science, Zunyi Medical University, Xinpu New District Campus No. 1 Street, Zunyi 563000, China

[9] Guizhou Key Laboratory of Anesthesia and Organ Protection, Zunyi Medical University, Xinpu New District Campus No. 1 Street, Zunyi 563000, China